Stability Analysis of Composite Laminates With and Without Cutout.

A Thesis Submitted
in Partial Fulfillment of the Requirements
for the Degree of
Master of Technology

by

Anil Valavala

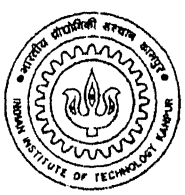

to the

Department of Aerospace Engineering
Indian Institute of Technology, Kanpur

September, 2004

CERTIFICATE

This is certify that the work contained in the thesis entitled " *Stability Analysis of Composite Laminates With and Without Cutouts*", by *Anil Valavala*, has been carried out under our supervision and that this work has not been submitted else where for a degree.

C.S. Upadhyay
Dr.C.S.Upadhyay
Asst.Professor,
Department Of Aerospace Engineering,
Indian Institute Of Technology,
Kanpur-208016.

N.G.R. Iyengar
Dr. N.G.R.Iyengar
Professor,
Department Of Aerospace Engineering,
Indian Institute Of Technology,
Kanpur-208016.

August, 2004.

Acknowledgements

I take this immense opportunity to express my sincere gratitude to my thesis supervisors Dr. N.G.R.Iyengar and Dr. C.S Upadhyay for their invaluable guidance, unstinted support and constant encouragement. It would never have been possible for me to complete this work without their valuable suggestions, innovative ideas and their patience. I really enjoyed my work and its been an enlightening experience working under my esteemed supervisors. I am very much indebted to them for their valuable discussions which helped me to develop independent thinking in me.

I also take this opportunity to express my regards to Dr. C.Venkatesan and Dr. D.Yadav for the invaluable knowledge they have imparted to me in Aerospace Engineering. I extend my thanks to the technical staff of Aerospace department for providing a good working enviroment.

Words are not sufficient to express my gratitude for the love and affection from my parents, brother and sister. I will never forget the struggle my parents had taken to bring me here. I am indebted to my buddies vishy, gita, jahnavi, bhanu and ravi for their love, encouragement and support at all times.

Life in IITK is memorable in the company of my dearest friends paparao, rohini, kiran, sushma, qureshi, raogaru, kalyan, ksvreddy, mallesh, annayya, babu, satya, shiva, krishna, seenu and gautham . I enjoyed each and every moment spent with them. I would never forget my association with ashoke and ishaq, who used to motivate me always. I am very thankful for all my structure labmates mohite, amit, rupal, laxman, nagendra, sateesh, abhiram, nilesh and atul for their help and concern. I am also thankful to bhavani, who used to be with me whenever I call him. And also my due thanks to Mr.Alok Gupta for solving my software problems at times. And last but not the least, I thank all my hall-4 friends for making my stay in IITK a pleasant one.

Abstract

Composites offer unique opportunities in aerospace design. Apart from being lighter the structural performance offered by it far more versatile than can obtained with the conventional materials. Composite plates with holes and cutouts are extensively used in aerospace structures. Cutouts change the mechanical behavior of composite plates. Hence the stability analysis of such plate structures is very essential for understanding the behavior of systems under different loadings.

In the present study an attempt has been made to take into account the effects of the cutouts in a moderately thick/very thick composite laminated plates under in-plane, compressive and shear loading using "Simple Higher Order Shear Deformation Theory" based on four unknown displacement functions instead of five, which is commonly used for most of the other higher order theories.The finite element method is employed to study the buckling load. A C^1 continuous shear flexible finite element based on the HSDT model is developed using the Hermite cubic polynomial for the rectangular element. The plate geometry has been modeled using linear Lagrange rectangular elements and hence subparametric formulation has been adopted.

The analytical results obtained for a plate without a cutout have been compared with the results obtained by different theories. The change in buckling response of thick rectangular laminated plates with and without cutout with respect to the fibre orientation angles has been studied. The effect of the cutout dimensions to the plate dimensions on the buckling load is plotted for cross-ply laminate. The interaction curves for N_x and N_y and for N_x and N_{xy} with and without a cutout have been studied .

Contents

List of Tables

List of Figures

List Of Symbols

X, Y, Z	Caretsian coordinates
a, b, h	Length,width and thickness of the laminated plate
a/b	Aspect ratio of laminate
a/h	Length/thickness ratio of laminate
θ	Lamina orientation angle
NL	Number of layers
z_k	Thickness of k^{th} lamina
u, v, w	Displacements along X, Y and Z directions respectively
w_b, w_s	Components of transverse displacement w
$\{\delta\}$	Generalized displacement vector
$\{\bar{\delta}\}$	Element nodal displacement vector
$[Q_k]$	2 D - stiffness matrix for k^{th} lamina
$[\bar{Q}_k]$	Transformed stiffness matrix for k^{th} lamina
N_x, N_y, N_{xy}	In-plane stress resultants
M_x, M_y, M_{xy}	Stress couples
P_x, P_y, P_{xy}	Higher order stress couples
Q_x, Q_y	Transverse shear forces in the laminate
$[A_{ij}]$	Extensional stiffness matrix
$[B_{ij}]$	Bending-extensional coupling matrix
$[D_{ij}]$	Bending stiffness matrix
$[E_{ij}]$	Higher order stiffness matrix
$[F_{ij}]$	Higher order stiffness matrix
$[G_{lm}]$	Transverse shear rigidity matrix
$[H_{ij}]$	Higher order stiffness matrix
$[D_r]$	Overall stiffness matrix
$\{\epsilon_0\}$	Mid-surface strains
$\{\kappa_0\}$	Mid-surface bending and twisting curvatures
$\{\kappa_l\}$	Higher order terms
$\{\gamma\}$	Transverse shear slope
N_i	Element shape functions in global co-ordinates

N_i'	Element shape functions in local co-ordinates
$\hat{N}_i'$	Element shape functions in natural co-ordinates
$\bar{a}, \bar{b}$	Length and width of rectangular element in local co-ordinate
Π	Total potential
U	Internal strain energy
T	Work done due to inplane loads
$[\bar{K}]$	Overall stiffness matrix
$[K]$	Elastic stiffness matrix
$[K_g]$	Geometric stiffness matrix
λ_{min}	Scaled initial buckling load
$\bar{N}_x, \bar{N}_y, \bar{N}_{xy}$	Nondimensionalized initial buckling loads

Chapter 1

Introduction

Structural materials can be broadly divided into four basic categories:metals, polymers, ceramics and composites. The word composite literally means consisting of two or more distinct parts. Thus a material which consists of two or more distinct materials combined in a macroscopic scale is called a composite. Common materials which can be included in this broad definition include reinforced concrete, fibre reinforced plastic, plywood, etc. Among the two phases one acts as as a binder or matrix and the other acts as a reinforcement.

Composites are generally used in structural components because they have desirable properties which could not be achieved by either of the constituent materials acting alone. The most common example is the fibrous composite consisting of reinforcing fibres embedded in a binder, or matrix material. Particle or flake reinforcements are also used but they are not so effective as fibres. Thus, in describing a composite material as a system, besides specifying the constituent materials and their properties, one needs to specify the geometry of the reinforcement with reference to the system. The geometry of the reinforcement may be described by the size, shape and size distribution.

Broadly composites can be classified into two categories:

1. Particle-reinforced composites.

2. Fibre-reinforced composites.

In the present investigation laminated fibrous composite is considered. Some of the commonly used fibre materials are E-glass, S-glass, Kevlar , Graphite, Boron, Silica, Tungsten etc. Fibres are used to provided the necessary strength and stiffness. Matrix materials (Polymers) can be classified into two types depending on their structure and thermal behaviour. These are namely:

1. Thermoplastic Polymers -Soften and melt on heating. Polyethylene, Polystyrene, Nylon, Placentals belong to this group.

2. Thermosetting Polymers-Do not soften but decompose on heating. Once solidified by a cross-linking curing process, they cannot be reshaped. Common examples of this kind include Epoxies, Polyesters, Phenolic, Silicone etc.

The main advantage of Polymeric matrix are low cost, easy processibility, good chemical resistance and low specific gravity.

Composites offers unique opportunities in design. Apart from being lighter it is a good substitute for conventional metallic materials. The structural performance offered by it is far more versatile than can be realized with conventional materials. An in-depth understanding of the principles governing their structural behaviour can help us explore this versatility to a maximum possible extent.

1.1 Composite Plates with Cutouts

Composite plates with holes and cutouts are extensively used in aerospace structures. The holes and cutouts are made for saving weight, for accommodating fuel, hydraulic or electrical lines and for providing accessibility to other parts of structures. Most of the studies in the stability analysis of plates are dealt with plates which are continuous or complete. In reality most aerostructures are flawed (either a crack or a cutout) in some way. Cutouts change the mechanical behaviour of plates. Hence, the analysis of such plate structures is mush essential. Thus the stability analysis of structures with cutouts is of technical importance for understanding the behaviour of systems under different types of loadings. Despite the practical importance of

these structures with cutouts, the number of technical papers and reports dealing with the subjects are very limited due to the complexity involved.

1.2 Motivation

The key factor in utilizing the strength and uniqueness of laminated composite plates is the proper understanding of its structural response under different work load conditions. Plate-like subcomponents come in various forms such as a annular plate or a rectangular plate that has a cutout. The present study focuses on the rectangular or square plates that have cutouts at different locations. Developing a thorough understanding of the behaviour of this subcomponent is a fundamental step towards understanding the behaviour of complex structures with cutouts such as airplane wing ribs. Knowledge of the basic response of the subcomponent provides useful information for the preliminary design of complex structures. In addition, this basic knowledge provides valuable insight into modelling complex structures with general purpose finite element codes, a step that takes place at a later phase in design process.

One behavioral aspect of the laminated composite plates which is vital for safe design is the initiation of buckling under the action of in-plane compressive and shear loads. Buckling can be termed as an unstable equilibrium of the body. The load at which an initially flat configuration of the plate under the action of in-plane forces suddenly changes to a bent configuration is known as initial buckling load. As the structure undergoes failure at this point it is imperative that a considerable amount of attention must be paid to find out its initial buckling load. The exact determination of this load governs the safe design process.

Most of the advanced composites in use have low transverse shear modulus (due to polymer matrices) compared to their in-plane moduli. Therefore, the classical theories of plates which predict the response characteristics of thin plates fairly accurately, may not yield accurate results for the similar configurations made up of composite materials. Thus, transverse shear deformation plays an important role in reducing the flexural stiffness of laminated composite plates. The classical plate

theory due to Poisson-Kirchoff neglected the transverse shear flexibility and assumed inextensible straight normals.This leads to an under-prediction of deflections and over-prediction of buckling loads.

So, for a better estimation of the initial buckling of composite laminated plates, many theories have been proposed over the years which include the effect of transverse shear deformation. The First order shear deformation theory due to Mindlin for thick plates assumes constant transverse shear strains through the thickness. As this theory allows only constant shear strain and does not satisfy the stress free conditions at the top and bottom surfaces of the plate, appropriate shear correction factors are introduced to achieve meaningful results. The exact evaluation of these shear correction factors is very difficult as it depends on the geometry and Poission's ratio. In recent years several simplified higher order shear deformation theories (HSDT) have been proposed, which not only allow parabolic variation of transverse shear strains but also satisfy the vanishing of transverse shear/strains at the bounding planes of the plate have been proposed. These higher order theories normally require five unknown displacement functions and requires C^0 continuous elements for finite element analysis. This requires numerical strategies such as reduced/selective integration to avoid shear locking effect (see [1]). A higher order theory proposed by Lim et al. [2] involves only four unknown displacement functions which requires C^1 continuous plate bending element and therefore does not necessitate numerical strategies to avoid shear locking effect. Also this theory involves lesser number of unknowns and is expected to be computationally more effective than the other theories which involve more unknowns.

1.3 Literature Survey

The advent of new strong and stiff fibre-reinforced composite materials approximately four decades ago revolutionized the structural applications in the aerospace industry. Since then, plates made of such materials are being extensively used in the industry. As a result various theories have been developed to understand the mechanical behaviour of composite laminates. Some of the studies ([3] and [4]) have

shown that the transverse shear effect is quite significant in the layered composite plates due to high ratio of in-plane elastic modulus to transverse shear modulus which made classical laminate plate theory unsuitable for the analysis. To overcome this difficulty a modified bending theory was formulated which accounts for the transverse shear deformation in isotropic plates. This plate bending theory is known as Reissner/Mindlin plate bending theory. This theory was applied for anisotropic plates by Whitney and Pagano (see [3] and [4]). In this theory the transverse shear strains are constant through the thickness of the plate. A shear correction factor has to be introduced to account for the discrepancy between the theory and the actual behaviour. Though this theory gives better results than classical laminate theory, the error in the solution increases as the plate thickness to side ratio increases. Thus to account for a better representation of the shear distribution across the thickness, Reddy [5] proposed a higher order shear deformation theory. A simplified higher order theory proposed by Lim et al. [2] involves only four unknowns instead of five for Reddy [5]. The simplified theory allows for the use of C^0 continuous plate bending element which is free from any shear locking effect. Singh [6] and Chakraborty [7] used this model for the response of laminated composite plates and beams.The stability of plates with perforated plates is studied by Yettram et al. [8]. They employed conjugate/load displacement method to analyse the structural stability of the perforated plates. They made the analysis on isotropic plates. Srivasta and Murti [9] presented a parametric study of the compression buckling behaviour of stress loaded composite plate with a central circular cutout. Jain and Kumar [10] analysed the postbuckling response of square laminates with a central circular/elliptical cutout. In their study, they investigated the large deflection behaviour and postbuckling behaviour of axially compressed square laminates with a circular and elliptical cutout. Prabhakara and Datta [11] studied the vibration and buckling behaviour of plates with centrally located cutouts. To the best of author's knowledge no results are available for the initial buckling analysis of laminated plates with rectangular cutout under uniaxial, biaxial compressive and shear in-plane loading in the published literature, using the simple higher order deformation theory.

1.4 Present Investigation

In the present investigation the following studies have been done.

1. Buckling behaviour of laminated composite plate without a cutout under in-plane compressive loading using simple higher order shear deformation theory as mentioned in section 1.3 is studied.The results are validated against those of other investigators.

2. Buckling behaviour of laminated composite plate with cutout under in-plane loading using simple higher order shear deformation theory.

3. The effect of various parameters like cutout size, plate aspect ratio, length to thickness ratio and fibre orientation on the initial buckling load of laminates.

4. Development of interaction curves for biaxial loading (N_x and N_y and N_x and $+N_{xy}$, N_x and $-N_{xy}$) of symmetric laminates for different cutout sizes, aspect ratio, length to thickness ratio and lamination angles. This will help in proper choice of laminate dimension.

1.5 Layout of Thesis

The thesis is broadly divided into five chapters.The details of thesis layout are presented here.

1. The first chapter is devoted to the the motivation for the present work, literature review, the focus of the present study and the layout of the thesis.

2. The second chapter discusses the plate model using higher order shear deformation theory, formulation of the problem and the laminate constitutive equations.

3. The third chapter deals with the finite element formulation of the present problem using energy principle.

4. Validation of the present model and several numerical results that detail the present investigation are presented in the fourth chapter.

5. The fifth chapter deals with the analysis of the results, concluding remarks and the further extension of the problem.

Chapter 2

Higher Order Plate Theory

2.1 Introduction

The classical theory of plates, in which it is assumed that normals to the mid-plane before deformation remain straight and normal to the plane after deformation, under-predicts deflections and over-predicts buckling loads. This is because the transverse shear strains are neglected in the classical theory. Many plate theories exist that account for transverse shear. Of these, the theories based on the assumed displacement field provide a background for the present theory. This chapter deals with the details of the plate theory proposed by Lim et al. [2] for isotropic plates and is extended to laminated composite plates.

The displacement field includes classical plate theory and first order shear deformation theory as subsets and accounts for parabolic variation of the transverse shear strains as well as the surface boundary conditions of zero transverse shear stresses (and hence shear strains) at the top and bottom surfaces of the plate. Hence there is no need to use shear correction coefficients in computations. The displacement field proposed by Reddy [5] is modified by reducing the number of variables to four (five, in case of Reddy's [5] theory). This simplification is based on the assumption that in-plane rotation tensor is constant through the thickness and the transverse displacement can be separated into two components in such a way that the transverse shear strains are functions of only one of these components.

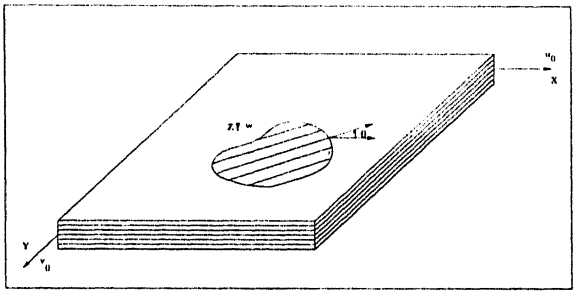

Figure 2.1: **Laminated plate with orientation of global co-ordinates**

2.2 Formulation of Displacement Field

The displacement field shown in Fig. 2.1 $u(x, y, z)$, $v(x, y, z)$ and $w(x, y, z)$ is represented as:

$$\begin{aligned} u(x,y,z) &= u_0(x,y) - zw_{b,x}(x,y) + z^2\phi_x(x,y) + z^3\psi_x(x,y); \\ v(x,y,z) &= v_0(x,y) - zw_{b,y}(x,y) + z^2\phi_y(x,y) + z^3\psi_y(x,y); \\ w(x,y,z) &= w_b(x,y) + w_s(x,y) \end{aligned} \tag{2.1}$$

where u_0, v_0 and w denote the displacements of a point $(x,\ y)$ on the midplane, and ψ_x and ψ_y are the warping of the normals to the midplane about the Y and X axes, respectively.The transverse displacement component w_b is such that its derivatives are numerically equal to the rotation of the cross-section (i.e. $\phi = -\nabla w_b$) and w_s is the displacement due to the effect of transverse shear deformation of the cross-section. The assumption that w_b and w_s are functions of x and y only is justified, since the transverse normal stress is of the order of $(h/a)^2$ times the in-plane normal stresses.

The von-Karman type nonlinear strain-displacement relationships for the higher

order theory under consideration can be written as follows:

$$\begin{aligned}
\epsilon_{xx} &= u_{0,x} + \tfrac{1}{2}(w_{b,x} + w_{s,x})^2 - z w_{b,xx} + z^2\phi_{x,x} + z^3\psi_{x,x};\\
\epsilon_{yy} &= v_{0,y} + \tfrac{1}{2}(w_{b,y} + w_{s,y})^2 - z w_{b,yy} + z^2\phi_{y,y} + z^3\psi_{y,y};\\
\epsilon_{zz} &= 0;\\
\gamma_{xy} &= u_{0,y} + v_{0,x} + (w_{b,x} + w_{s,x})(w_{b,y} + w_{s,y}) - 2z w_{b,xy}\\
&\quad + z^2(\phi_{y,x} + \phi_{x,y}) + z^3(\psi_{y,x} + \psi_{x,y});\\
\gamma_{xz} &= w_{s,x} + 2z\phi_x + 3z^2\psi_x;\\
\gamma_{yz} &= w_{s,y} + 2z\phi_y + 3z^2\psi_y;
\end{aligned} \tag{2.2}$$

where comma (,) denotes the partial derivatives.

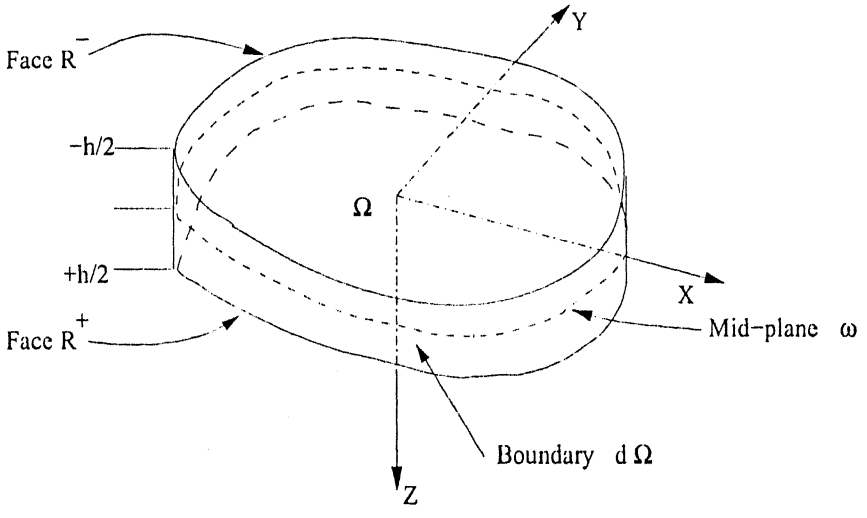

Figure 2.2: **Representation of arbitrary three dimensional domain**

The surface boundary condition that the transverse shear stresses vanish on the plate's top and bottom faces (Fig. 2.2) is equivalent to the requirement that the corresponding strains be zero on these surfaces, i.e.

$$\gamma_{xz}(x, y, \pm\tfrac{h}{2}) = \gamma_{yz}(x, y, \pm\tfrac{h}{2}) = 0$$

On introduction of the conditions as given above in the expressions for transverse shear strains (from Eq. 2.2), the following relations are obtained

$$\begin{aligned}
&\phi_x = \phi_y = 0 \quad \text{and}\\
&\psi_x = -\tfrac{4}{3h^2} w_{s,x} \; ; \quad \psi_y = -\tfrac{4}{3h^2} w_{s,y}
\end{aligned} \tag{2.3}$$

The displacement field of Eq. (2.1) is modified by setting ϕ_x and ϕ_y to be zero according to conditions of Eq. (2.3). The resulting displacement field is given as :

$$\begin{aligned} u(x,y,z) &= u_0(x,y) - zw_{b,x}(x,y) - \tfrac{4z^3}{3h^2}w_{s,x}(x,y); \\ v(x,y,z) &= v_0(x,y) - zw_{b,y}(x,y) - \tfrac{4z^3}{3h^2}w_{s,y}(x,y); \\ w(x,y,z) &= w_b(x,y) + w_s(x,y); \end{aligned} \tag{2.4}$$

In Eq. (2.4) u, v and w are the displacements along x, y and z directions respectively. u_0, v_0 and w (w_b and w_s) are the mid-plane displacements. Thus, the generalized displacement vector $\{\delta\}$ of the mid-surface contains four degrees of freedom (DOF) and is given by:

$$\{\delta\} = \{u_0, v_0, w_b, w_s\}^T.$$

The corresponding strain-displacement relationships are:

$$\begin{aligned} \epsilon_{xx} &= u_{0,x} + \tfrac{1}{2}(w_{b,x} + w_{s,x})^2 - zw_{b,xx} - \tfrac{4z^3}{3h^2}w_{s,xx}; \\ \epsilon_{yy} &= v_{0,y} + \tfrac{1}{2}(w_{b,y} + w_{s,y})^2 - zw_{b,yy} - \tfrac{4z^3}{3h^2}w_{s,yy}; \\ \epsilon_{zz} &= 0; \\ \gamma_{xy} &= u_{0,y} + v_{0,x} + (w_{b,x} + w_{s,x})(w_{b,y} + w_{s,y}) - 2zw_{b,xy} \\ &\quad - \tfrac{8z^3}{3h^2}w_{s,xy}; \\ \gamma_{xz} &= (1 - \tfrac{4z^2}{h^2})w_{s,x}; \\ \gamma_{yz} &= (1 - \tfrac{4z^2}{h^2})w_{s,y}; \end{aligned} \tag{2.5}$$

It can be noted that these kinematic relationships can be obtained by substituting $\psi_x = -w_{b,x}, \psi_y = -w_{b,y}$ and $w = w_b + w_s$ in Reddy's [5] higher order theory involving five unknowns $(u_0, v_0, w_0, \psi_x, \psi_y)$.

It can be shown that the present formulation degenerates to first order shear deformation theory by suitably dropping higher order terms and incorporating appropriate shear correction factors (for isotropic plate whose value is 5/6). The classical laminate theory (CLT) can be derived from the present theory by equating w_s to zero.

The strain-displacement relationships given in Eq. (2.2) can be rewritten as:

$$\begin{aligned}
\epsilon_{xx} &= \epsilon_{0x} + z\kappa_{0x} + z^3\kappa_{lx}; \\
\epsilon_{yy} &= \epsilon_{0y} + z\kappa_{0y} + z^3\kappa_{ly}; \\
\epsilon_{zz} &= 0; \\
\gamma_{xy} &= \gamma_{0xy} + z\kappa_{0xy} + z^3\kappa_{lxy}; \\
\gamma_{xz} &= (1 - \frac{4z^2}{h^2})w_{s,x}; \\
\gamma_{yz} &= (1 - \frac{4z^2}{h^2})w_{s,y};
\end{aligned} \tag{2.6}$$

where :

$$\begin{array}{lll}
\epsilon_{0x} = u_{0,x}; & \epsilon_{0y} = v_{0,y}; & \gamma_{0xy} = u_{0,y} + v_{0,x}; \\
\kappa_{0x} = -w_{b,xx}; & \kappa_{0y} = -w_{b,yy}; & \kappa_{0xy} = -2w_{b,xy}; \\
\kappa_{lx} = -\frac{4}{3h^2}w_{s,xx}; & \kappa_{ly} = -\frac{4}{3h^2}w_{s,yy}; & \kappa_{lxy} = -\frac{8}{3h^2}w_{s,xy}
\end{array}$$

2.3 Laminate Constitutive Equations

A single layer of a laminated composite material is generally referred to as a ply or lamina. A lamina (considered a unidirectional composite) is characterized by having all fibres (either a single ply or multiple plies) oriented in the same direction. This model allows one to treat the lamina as an orthotropic material whose material symmetry planes are parallel and transverse to the fibre direction. The model used to represent a lamina consists of unidirectional fibres per layer which is further assumed as perfectly straight and uniformly oriented within the lamina.

The following figure represents a laminate with the material co-ordinates axes L and T defined parallel and perpendicular to the fiber direction respectively. X, Y and Z represents the global co-ordinates. The material co-ordinate axis T' is assumed to be along Z axis. The angle between global co-ordinate axis X and material co-ordinate axis L is θ and is known as the fibre orientation angle. As a sign convention anti-clockwise angle from $+ve\ X$ direction is taken as positive.

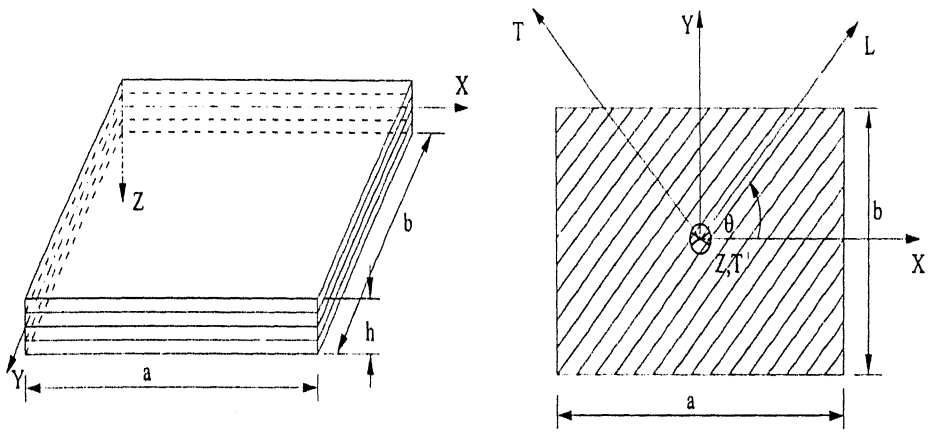

Figure 2.3: **Co-ordinate axes for the lamina**

2.4 Generalised Hooke's law

In the derivation of the laminate constitutive equations the following two assumptions are made.

1. The lamina is a continuum.
2. It behaves as a linearly elastic material

Further at the micro-level the following assumptions are made about the material.

1. Perfect bonding exists between the fibres and matrix.
2. Fibres are parallel and distributed uniformly throughout the laminate.
3. The matrix is free of voids or micro cracks and is initially in a stress free state.
4. Both fibres and matrix are isotropic and obey Hooke's law.

Stress-strain relations for the k^{th} lamina in the material co-ordinate axes,whose fibres are oriented at an angle θ with reference to the X axis is given as (see[11]):

$$\{\sigma_i\}_k = [Q_{ij}]_k\{\epsilon_j\}_k \tag{2.7}$$

where $\{\sigma_i\}$ is the vector of stress components, $[Q_{ij}]_k$ is the 2 D - stiffness matrix with respect to material co-ordinate axes, and $\{\epsilon_j\}$ are the engineering strain components for the k^{th} lamina.

In the expanded form, the above relation can be written as :

$$\begin{Bmatrix} \sigma_L \\ \sigma_T \\ \tau_{LT} \\ \tau_{LT'} \\ \tau_{TT'} \end{Bmatrix}_k = \begin{bmatrix} Q_{11} & Q_{12} & 0 & 0 & 0 \\ Q_{21} & Q_{22} & 0 & 0 & 0 \\ 0 & 0 & Q_{66} & 0 & 0 \\ 0 & 0 & 0 & Q_{44} & 0 \\ 0 & 0 & 0 & 0 & Q_{66} \end{bmatrix}_k \begin{Bmatrix} \epsilon_L \\ \epsilon_T \\ \gamma_{LT} \\ \gamma_{LT'} \\ \gamma_{TT'} \end{Bmatrix}_k \tag{2.8}$$

where :

$$Q_{11} = \frac{E_L \nu_{tt}}{(1 - \nu_{LT}\nu_{TL})}; \qquad Q_{12} = Q_{21} = \frac{E_T \nu_{LT}}{(1 - \nu_{LT}\nu_{TL})};$$
$$Q_{22} = \frac{E_T}{(1 - \nu_{LT}\nu_{TL})}; \qquad Q_{66} = G_{LT};$$
$$Q_{44} = G_{LT'}; \qquad Q_{55} = G_{TT'};$$

The stress and strains in the X, Y and Z directions are obtained by the transformation of the relations given in Eq. (2.7). The transformed stress strain relations for the k_{th} lamina are given as:

$$\begin{Bmatrix} \sigma_x \\ \sigma_y \\ \tau_{xy} \\ \tau_{xz} \\ \tau_{yz} \end{Bmatrix}_k = \begin{bmatrix} \bar{Q}_{11} & \bar{Q}_{12} & \bar{Q}_{16} & 0 & 0 \\ \bar{Q}_{12} & \bar{Q}_{22} & \bar{Q}_{26} & 0 & 0 \\ \bar{Q}_{16} & \bar{Q}_{26} & \bar{Q}_{66} & 0 & 0 \\ 0 & 0 & 0 & \bar{Q}_{44} & \bar{Q}_{45} \\ 0 & 0 & 0 & \bar{Q}_{45} & \bar{Q}_{55} \end{bmatrix}_k \begin{Bmatrix} \epsilon_x \\ \epsilon_y \\ \gamma_{xy} \\ \gamma_{xz} \\ \gamma_{yz} \end{Bmatrix}_k \tag{2.9}$$

where:

$$
\begin{aligned}
\bar{Q}_{11} &= Q_{11}c^4 + (2Q_{12} + 4Q_{66})s^2c^2 + Q_{22}s^4; \\
Q_{12} &= Q_{12}(s^4c^4) + (Q_{11} + Q_{12} - 4Q_{66})s^2c^2; \\
\bar{Q}_{16} &= (Q_{11} - Q_{12} + 2Q_{66})sc^3 + (Q_{12} - Q_{22} + 2Q_{66})s^3c; \\
\bar{Q}_{22} &= Q_{11}s^4 + (2Q_{12} + 4Q_{66})s^2c^2 + Q_{22}c^4; \\
\bar{Q}_{26} &= (Q_{11} - Q_{12} - 2Q_{66})s^3c + (Q_{12} - Q_{22} + 2Q_{66})sc^3; \\
\bar{Q}_{66} &= (Q_{11} - 2Q_{12} + Q_{22} - 2Q_{66})s^2c^2 + Q_{66}(c^4 + s^4); \\
\bar{Q}_{44} &= Q_{44}c^2 + Q_{55}s^2; \\
\bar{Q}_{45} &= (Q_{44} - Q_{55})cs; \\
\bar{Q}_{55} &= Q_{55}c^2 + Q_{44}s^2;
\end{aligned}
$$

where, $[\bar{Q}_{ij}]$ is the transformed stiffness matrix, c = $\cos\theta$ and s = $\sin\theta$ with θ denoting the angle of orientation of the k_{th} lamina.

Using the above lamina constitutive equations and integrating the stresses over the laminate thickness, the stress resultants, stress couples, transverse shear resultants and higher order stress couples per unit length, for a laminate with NL laminae are,

$$
\begin{Bmatrix} \{\mathbf{N_i}\} \\ \{\mathbf{M_i}\} \\ \{\mathbf{P_i}\} \\ \{\mathbf{Q_l}\} \end{Bmatrix} = \begin{bmatrix} [A_{ij}] & [B_{ij}] & [E_{ij}] & [0] \\ [B_{ij}] & [D_{ij}] & [F_{ij}] & [0] \\ [E_{ij}] & [F_{ij}] & [H_{ij}] & [0] \\ [0] & [0] & [0] & [G_{lm}] \end{bmatrix} \begin{Bmatrix} \{\epsilon_{0j}\} \\ \{\kappa_{0j}\} \\ \{\kappa_{lj}\} \\ \{\gamma_m\} \end{Bmatrix} \qquad (2.10)
$$

$$
\begin{matrix} (\mathrm{i}\ ,\ \mathrm{j} = 1\ ,\ 2 \text{ and } 6) \\ (\mathrm{l}\ ,\ \mathrm{m} = 4\ ,\ 5) \end{matrix}
$$

(Detailed expansion of Eq. (2.9) is given in Appendix A.)
where $\{\epsilon_0\}$ are the mid-surface strains, $\{\kappa_0\}$ are the mid-surface bending and twisting curvatures, $\{\kappa_l\}$ are the higher order terms and $\{\gamma\}$ are the transverse shear slope

and

$$\{\mathrm{N_i}\}^{\mathrm{T}} = (N_x, N_y, N_{xy}) = \sum_{k=1}^{NL} \int_{z_k}^{z_{k-1}} (\sigma_x, \sigma_y, \tau_{xy})^k \quad dz; \tag{2.11}$$

$$\{\mathrm{M_i}\}^{\mathrm{T}} = (M_x, M_y, M_{xy}) = \sum_{k=1}^{NL} \int_{z_k}^{z_{k-1}} (\sigma_x, \sigma_y, \tau_{xy})^k \; z \; dz; \tag{2.12}$$

$$\{\mathrm{P_i}\}^{\mathrm{T}} = (P_x, P_y, P_{xy}) = \sum_{k=1}^{NL} \int_{z_k}^{z_{k-1}} (\sigma_x, \sigma_y, \tau_{xy})^k \; z^3 \; dz; \tag{2.13}$$

$$\{\mathrm{Q_i}\}^{\mathrm{T}} = (Q_x, Q_y) = \sum_{k=1}^{NL} \int_{z_k}^{z_{k-1}} (\tau_{xz}, \tau_{yz})^k \; (1 - \frac{4z^2}{h^2}) \; dz; \tag{2.14}$$

Here, z_i are the z coordinates corresponding to the laminae interfaces as shown in Fig. 2.4.

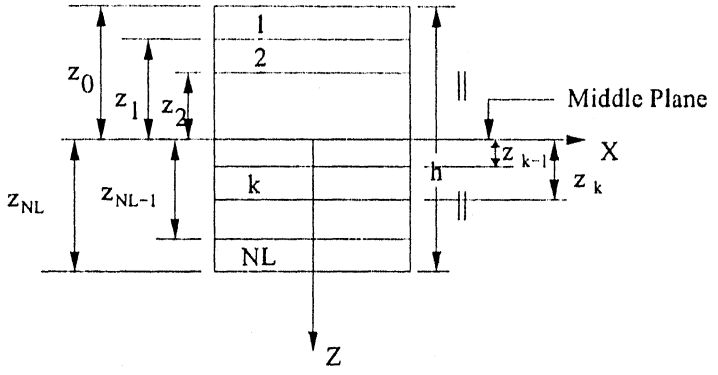

Figure 2.4: **Geometry of multi layered laminate**

Thus, with the assumed displacement model, the various stiffness matrices derived are:

$[A_{ij}]$ = Extensional; $[B_{ij}]$ = Bending-extensional coupling;
$[D_{ij}]$ = Bending; $[G_{lm}]$ = Transverse shear stiffness and
$[E_{ij}]$, $[F_{ij}]$, $[H_{ij}]$ = Higher order stiffnesses.

The set of stiffness matrices $[A_{ij}]$, $[B_{ij}]$, $[D_{ij}]$, $[E_{ij}]$, $[F_{ij}]$, $[H_{ij}]$ and $[G_{lm}]$ are used in forming overall stiffness matrix $[D_r]$ for the laminate (for details see [7]).

Chapter 3

Finite Element Formulation

This chapter deals with the finite element formulation of the problem under consideration. Four noded rectangular elements are used to represent the total domain of the plate. To satisfy the continuity of the slope, Hermite cubic interpolations are used in the approximation. A C^1 continuous shear flexible element based on the presented higher order theory is developed using the Hermite interpolation formulae as indicated by Bogner et al. [13]. The geometry of the plate is modelled using the linear Lagrange interpolation functions. A typical mesh generated over the plate domain with and without a centrally located cutout is shown in Figs 3.1.and 3.2. The details of the finite element formulation is presented below.

3.1 Definition

Let V be the displacement vector defined as:

$$\left\{ V \right\} = \left\{ \begin{array}{c} u \\ v \\ w \end{array} \right\} \tag{3.1}$$

The stress and strain vectors corresponding to $\{V\}$ be $\{\sigma\}$ and $\{\epsilon\}$ and can be defined as:

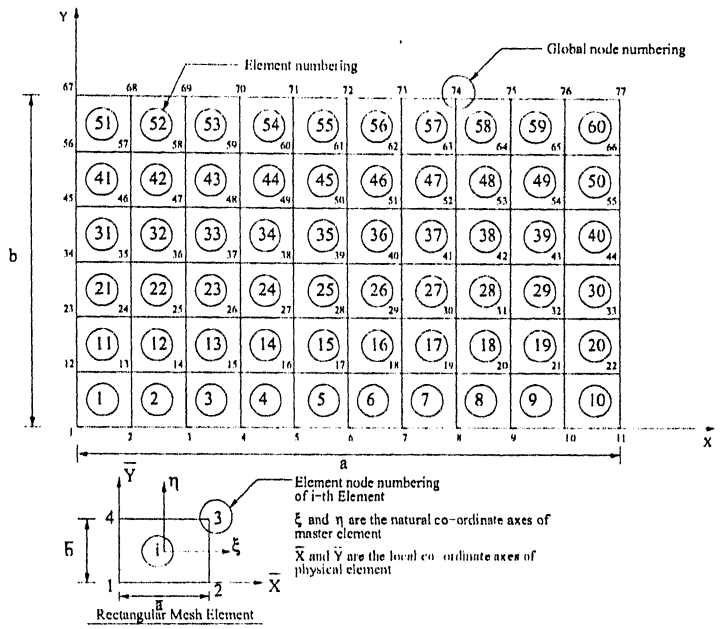

Figure 3.1: **Typical mesh of Rectangular plate domain**

$$\left\{ \sigma \right\} = \begin{Bmatrix} \sigma_x \\ \sigma_y \\ \tau_{xy} \\ \tau_{xz} \\ \tau_{yz} \end{Bmatrix} \qquad \epsilon = \begin{Bmatrix} \epsilon_x \\ y \\ \gamma_{xy} \\ \gamma_{xz} \\ \gamma_{yz} \end{Bmatrix} \tag{3.2}$$

From the generalized Hooke's law which relates the stress components to the respective strain components in global coordinate system:

$$\{\sigma\} = [\bar{Q}]\{\epsilon\} \tag{3.3}$$

The material stiffness matrix $[\bar{Q}]$ for orthotropic material is given in Eq. (2.8) for each lamina.

We are concerned with the initial buckling of the laminate. Hence, the non-linear terms in the strain-displacement relationships as described in Eq. (2.5) are neglected

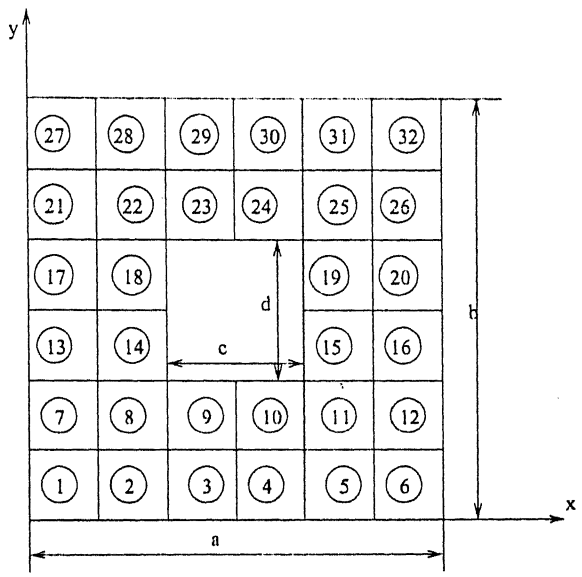

c is the length of the cutout
d is the width of the cutout

Figure 3.2: **Typical mesh of Rectangular plate domain with a cutout**

for our study because the transverse deflection (both w_b and w_s) is assumed to be very small.

The linear strain-displacement relationships can be written as:

$$\begin{aligned}
\epsilon_{xx} &= u_{0,x} - z\, w_{b,xx} - \tfrac{4}{3}\tfrac{z^3}{h^2}\, w_{s,xx};\\
\epsilon_{yy} &= v_{0,y} - z\, w_{b,yy} - \tfrac{4}{3}\tfrac{z^3}{h^2}\, w_{s,yy};\\
\epsilon_{zz} &= 0;\\
\gamma_{xy} &= u_{0,y} + v_{0,x} - 2\, z\, w_{b,xy} - \tfrac{8}{3}\tfrac{z^3}{h^2}\, w_{s,xy};\\
\gamma_{xz} &= (1 - \tfrac{4}{h^2}\tfrac{z^2}{h^2})\, w_{s,x};\\
\gamma_{yz} &= (1 - \tfrac{4}{h^2}\tfrac{z^2}{h^2})\, w_{s,y};
\end{aligned} \tag{3.4}$$

The above relations are expressed in matrix form as :

$$\{\epsilon\} = [\bar{D}]\,\{V\} \tag{3.5}$$

where $[\bar{D}]$ is the differential operator in terms of global coordinates, defined as

$$[\bar{D}] = \begin{Bmatrix} \frac{\partial}{\partial x} & 0 & 0 \\ 0 & \frac{\partial}{\partial y} & 0 \\ \frac{\partial}{\partial y} & \frac{\partial}{\partial x} & 0 \\ \frac{\partial}{\partial z} & 0 & \frac{\partial}{\partial x} \\ 0 & \frac{\partial}{\partial z} & \frac{\partial}{\partial y} \end{Bmatrix} \tag{3.6}$$

The components of displacement can be expressed in terms of the four unknowns, which can be written as:

$$\{\delta\}^T = \{u_0, v_0, w_b, w_s\} \tag{3.7}$$

For any element the field variables can be written in terms of shape functions and nodal variables as:

$$\begin{aligned}
u_0(x,y) &= \sum_{i=1}^{4} N_i' \, u_{0i} + \sum_{i=1}^{4} N_{i+4}' \, u_{0,xi} + \sum_{i=1}^{4} N_{i+8}' \, u_{0,y_i} + \\
&\quad \sum_{i=1}^{4} N_{i+12}' \, u_{0,xy_i}; \\
v_0(x,y) &= \sum_{i=1}^{4} N_i' \, v_{0i} + \sum_{i=1}^{4} N_{i+4}' \, v_{0,xi} + \sum_{i=1}^{4} N_{i+8}' \, v_{0,y_i} + \\
&\quad \sum_{i=1}^{4} N_{i+12}' \, v_{0,xy_i}; \\
w_b(x,y) &= \sum_{i=1}^{4} N_i' \, w_{bi} + \sum_{i=1}^{4} N_{i+4}' \, w_{b,xi} + \sum_{i=1}^{4} N_{i+8}' \, w_{b,y_i} + \\
&\quad \sum_{i=1}^{4} N_{i+12}' \, w_{b,xy_i}; \\
w_s(x,y) &= \sum_{i=1}^{4} N_i' \, w_{si} + \sum_{i=1}^{4} N_{i+4} \, w_{s,xi} + \sum_{i=1}^{4} N_{i+8}' \, w_{s,y_i} + \\
&\quad \sum_{i=1}^{4} N_{i+12}' \, w_{s,xy_i}
\end{aligned} \tag{3.8}$$

In the above expression u_{0i}, $u_{0,xi}$, u_{0,y_i},u_{0,xy_i}, v_{0i}, $v_{0,xi}$, v_{0,y_i}, v_{0,xy_i}, w_{bi}, $w_{b,xi}$, w_{b,y_i}, w_{b,xy_i}, w_{si}, $w_{s,xi}$, w_{s,y_i}, w_{s,xy_i} $(i = 1,4)$ are the sixteen degrees of freedom

per node, N_i's are the element shape functions in local co-ordinates (in terms of $\bar{X}$ and $\bar{Y}$ as shown in Fig.3.2). In natural co-ordinates (in terms of ξ and η as shown in Fig.3.2) N_i's can be expressed as $\hat{N}_i'$s (see [1]). Substituting Eq. (3.7) in

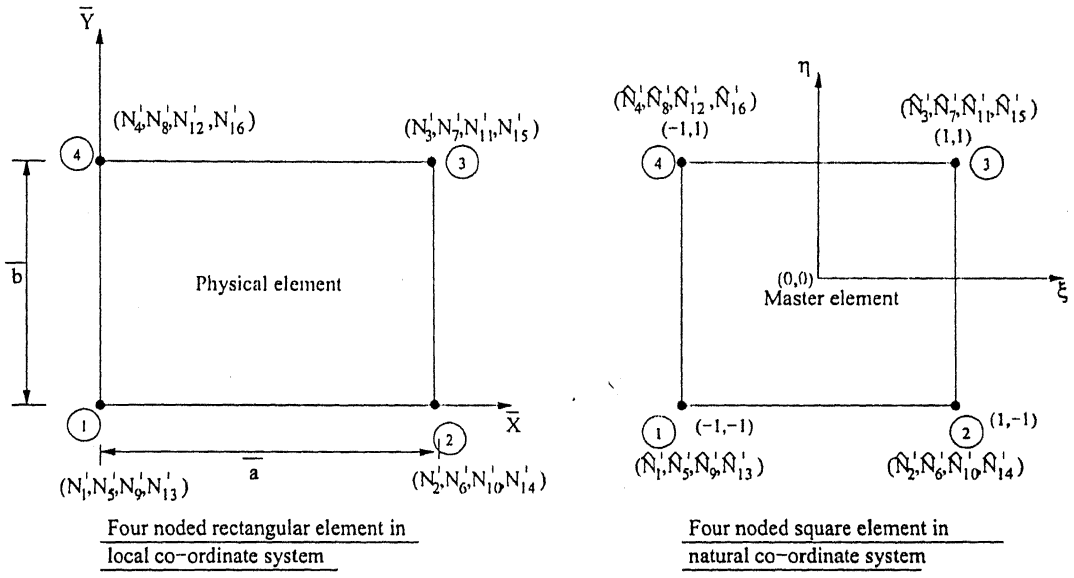

Figure 3.3: **Four noded rectangular element**

the strain-displacement relations given in Eq. (3.4) the following relations can be established:

$$\begin{Bmatrix} \epsilon_{0x} \\ \epsilon_{0y} \\ \gamma_{0xy} \\ \kappa_{0x} \\ \kappa_{0y} \\ \kappa_{0xy} \\ \kappa_{lx} \\ \kappa_{ly} \\ \kappa_{lxy} \\ w_{s,x} \\ w_{s,y} \end{Bmatrix}_{11\times 1} = [B_0]_{11\times 64}\,\{\bar{\delta}\}_{64\times 1} \tag{3.9}$$

where:

$\{\bar{\delta}\}^T = \{\ u_{0i},\ u_{0,x_i},\ u_{0,y_i},\ u_{0,xyi},\ v_{0i},\ v_{0,x_i},\ v_{0,y_i},\ v_{0,xy_i},\ w_{bi},\ w_{b,xi},\ w_{b,y_i},\ w_{b,xy_i},\ w_{si},$
$w_{s,xi},\ w_{s,y_i},\ w_{s,xy_i}\}$; $(i = 1,...,4)$
and:

$$\epsilon_{0x} = u_{0,x}; \quad \epsilon_{0y} = v_{0,y}; \quad \gamma_{0xy} = u_{0,y} + v_{0,x};$$
$$\kappa_{0x} = -w_{b,xx}; \quad \kappa_{0y} = -w_{b,yy}; \quad \kappa_{0xy} = -2w_{b,xy};$$
$$\kappa_{lx} = -\tfrac{4}{3h^2}\, w_{s,xx}; \quad \kappa_{ly} = -\tfrac{4}{3h^2}\, w_{s,yy}; \quad \kappa_{lxy} = -\tfrac{8}{3h^2}\, w_{s,xy}$$

The details of $[B_0]$ are given in Appendix B.

3.2 Finite Element Formulation

An eigen value buckling analysis is a linearized form of a geometrically nonlinear formulation, useful for estimating the limits of elastic stability.

The undeformed configuration of the plate is denoted by Ω and its boundary by $\partial\Omega$. The infinitesimal strain is defined in terms of the Cartesian components of the displacements ($u_i, i = 1,2,3$):

$$\epsilon_{ij} = \frac{1}{2}\,(\,u_{i,j} + u_{j,i}\,)$$

which is a simplification of the Green-Lagrange strains defined by

$$\Xi_{ij} = \epsilon_{ij} + \frac{1}{2}\,(\,u_{\alpha,i} \times u_{\alpha,j}\,)$$

The simplification is justified by the assumption that $|u_{ij}| << 1$ and hence the product terms $u_{\alpha,i}u_{\alpha,j}$ are negligible in relation to $u_{i,j}$. The stress-strain relationship is:

$$\sigma_{ij} = {\sigma_{ij}}^0 + C_{ijkl}\,\epsilon_{kl}$$

where σ^0_{ij} is a pre-existing stress state, independent of u_i, and C_{ijkl} is the tensor of the elastic moduli of the material. An important property of σ^0_{ij} is that, it is in equilibrium with the corresponding tractions $T^0_i = \sigma^0_{ij}\, n_j$ in the sense: [see [14]]

$$\frac{1}{2}\int_\Omega \sigma^0_{ij}\,(\,v_{i,j} + v_{j,i})\,dV = \int_{\partial\Omega} T^0_i\, v_i\, dA \quad for\ all\ v_i \in E\,(\Omega)$$

where dV and dA represent the differential volume and differential area respectively, and $E(\Omega)$ is the space of kinematically admissible perturbations. When the reference configuration is stress-free (i.e., $\sigma_{ij}^0 = 0$) then the potential energy is defined by:

$$\Pi(u) = \frac{1}{2}\int_\Omega C_{ijkl}\,\epsilon_{ij}\,\epsilon_{kl}\,dV - \int_{\partial\Omega} T_i\,u_i\,dA \tag{3.10}$$

The exact solution minimizes Π on the set of all kinematically admissible functions denoted by $\widetilde{E}(\Omega)$. When the reference configuration is not stress-free then the work done by σ_{ij}^0 due to the nonlinear strain terms may not be negligible. Therefore the potential energy expression is written in the following form.

$$\Pi(u) = \frac{1}{2}\int_\Omega C_{ijkl}\,\epsilon_{ij}\,\epsilon_{kl}\,dV + \frac{1}{2}\int_\Omega \sigma_{ij}^0\,u_{\alpha,i}\,u_{\alpha,j}\,dV - \int_{\partial\Omega} T_i\,u_i\,dA \tag{3.11}$$

The first integral in the above equation represents the internal strain energy and the second term represents the work done by the initial stresses due to the nonlinear strain terms. The work done by σ_{ij}^0 due to the linear strain terms is canceled by the work done by T_i^0 in the sense of Eq.(3.10).

The exact solution to this problem is obtained by minimizing the total potential energy Π. This can be obtained as:

$$\partial^{(1)}\,\Pi = 0 \tag{3.12}$$

which is also the *Virtual Work Formulation* of the problem in terms of the components of δ(and hence $\bar{\delta}$). This leads to the generalized finite element formulation which can be expressed as:

$$[\bar{K}]\,\{\bar{\delta}\} = \{F\} \tag{3.13}$$

Where $[\bar{K}]$ is the global stiffness matrix which is composed of two components (i.e. global elastic stiffness matrix $[K]$ and global geometric stiffness matrix $[K_g]$) and $\{F\}$ is the global load vector which is zero in our case since $W^{(e)} = 0$.
Hence Eq. (3.15) can be rewritten as:

$$\Big[\,[K] - [K_g]\,\Big]\,\{\bar{\delta}\} = 0 \tag{3.14}$$

In the following sections, we are going to employ the virtual work formulation to derive the finite element equations governing the initial buckling problem.

3.3 Deriving the Element Elastic Stiffness Matrix

The elastic stiffness matrix corresponding to assumed deformation state of an element can be defined by expressing the internal strain energy in terms of unknown nodal displacements. In the formulation of unsymmetric laminates the membrane, the flexure, membrane-flexure coupling and shear strains contribute to strain energy. The internal strain energy of an element (given by area A^e) can be expressed as:

$$U^e = \frac{1}{2}\int_{A^{(e)}} (N_x\,\epsilon_{0x} + N_{y\,0y} + N_{xy}\,\epsilon_{0xy} + M_x\,\kappa_{0x} + M_y\,\kappa_{0y} + M_{xy}\,\kappa_{0xy} + P_x\,\kappa_{lx} + P_y\,\kappa_{ly} + P_{xy}\,\kappa_{lxy} + Q_x\,w_{s,x} + Q_y\,w_{s,y})\,dA \tag{3.15}$$

The Eq. (3.8) along with Eq. (2.9) can be used to express the internal strain energy as:

$$U^e = \frac{1}{2}\int_{A^{(e)}} (\{\bar{\delta}^e\}^T\,[B_0^T]\;[D_r]\,[B_0]\,\{\bar{\delta}^e\})\;dA \tag{3.16}$$

The strain energy expression can be written in concise form as:

$$U^{(e)} = \frac{1}{2}\,\{\bar{\delta}^e\}^T\,[K^e]\,\{\bar{\delta}^e\} \tag{3.17}$$

where $[K^e]$ is the elastic stiffness matrix and $\{\bar{\delta}^e\}$ are the unknown displacements corresponding to the finite element solution in an element e . $[K^e]$ is given by:

$$[K^e] = \int_{A^{(e)}}\,[B_0]^T\,[D_r]\,[B_0]\,dA \tag{3.18}$$

Numerical integration is carried out to get the element elastic stiffness matrix.

3.4 Deriving the Element Geometric Stiffness Matrix

The total work done by the in-plane applied loads in an element can be expressed as:

$$T^e = \frac{1}{2}\int_{A^{(e)}} (\{\bar{\delta}^e\}^T\,[B_g^T]\;[N]\,[B_g]\,\{\bar{\delta}^e\})\;dA \tag{3.19}$$

T^e can be written in a concise form as:

$$T^{(e)} = \frac{1}{2}\,\{\bar{\delta}^e\}^T\,[K_g^e]\,\{\bar{\delta}^e\} \tag{3.20}$$

The details of $[B_g]$ is given in Appendix C.

whereas:

$$[\bar{N}] = \begin{bmatrix} N_x & N_{xy} \\ N_{xy} & N_y \end{bmatrix} \tag{3.21}$$

Assuming that forces N_x, N_y and N_{xy} are represented by certain expressions with a common factor λ, so that

$$N_x = \lambda \bar{N}_x, \; N_y = \lambda \bar{N}_y, \; N_{xy} = \lambda \bar{N}_{xy}$$

then:

$$[\bar{N}] = \lambda \begin{bmatrix} N_x & N_{xy} \\ N_{xy} & N_y \end{bmatrix} \tag{3.22}$$

or

$$[N] = \lambda \; [\; N]$$

where:

$$[\bar{N}] = \begin{bmatrix} \hat{N}_x & \hat{N}_{xy} \\ \hat{N}_{xy} & \hat{N}_y \end{bmatrix} \tag{3.23}$$

where $[K_g]$ is the geometric stiffness matrix and $\{\bar{\delta}^e\}$ are the unknown displacements corresponding to the finite element solution in an element e.

$[K_g^e]$ is given by:

$$[K_g^e] = \lambda \int_{A^{(e)}} [B_g]^T \; [\bar{N}] \; [B_g] \; dA; \tag{3.24}$$

or

$$[K_g^e] = \lambda \, [\bar{K}_g{}^e] \tag{3.25}$$

Numerical integration is carried out to get the element geometric stiffness matrix.

3.5 Methodology for Finding Initial Buckling Load

The main objective of the present analysis is to investigate the initial buckling load of the composite laminate under different boundary conditions, cutout sizes, location

of the cutout, fibre orientation angles, plate aspect ratio's etc. Since we are dealing with the physical stability of the system, this buckling problem is an eigen value problem which is described below.

From Eqns. (3.16),(3.20) and (3.23) we obtain the final FEM equation as follows:

$$\left[[K] - \lambda[\bar{K}_g] \right] \{\bar{\delta}\} = 0 \tag{3.26}$$

The above equation can be stated as "Assuming that the steady state solution of the problem is known,is there any other solution into which the system would bifurcate if it were slightly disturbed from it equlibrium position".

The characteristic equation of the above eigenvalue problem can be expressed as:

$$\left| [K] - \lambda[\bar{K}_g] \right| = 0 \tag{3.27}$$

Eq. (3.25) is solved using NAG ROUTINES to obtain the eigenvalues λ_i (i = 1,M) where M is the dimension of the matrices $[K]$ and $[\bar{K}_g]$ (and is equal to the total number of degrees of freedom of the problem). The minimum value of λ corresponds to the scaled initial buckling load from which we obtain the initial buckling load as follows:

$$N_x \text{ (or } N_y \text{ or } N_{xy} \text{)} = \lambda_{min} \hat{N}_x \text{ (or } \hat{N}_y \text{ or } \hat{N}_{xy} \text{)}$$

The corresponding eigenvector (which is also found using NAG ROUTINES) gives the mode shape (not the exact displacements) corresponding to the initial buckling load.

3.6 Geometric Approximation

3.6.1 Linear Mapping of Straight Edge Rectangular Elements

In any finite element formulation an accurate representation of the domains is very essential. Any domain can be represented using rectangular elements since the interpolation functions are easily derivable for them. Numerical integration schemes such as the Gauss-Legendre scheme require that the integral be evaluated on a specific domain or with respect to a specific co-ordinate system.The transformation of the geometry and the variable coefficients of the differential equation from the problem co-ordinates (x, y) to the co-ordinates (ξ, η) results in algebraically complex expressions and this precludes analytical (i.e., exact) evaluation of the integrals. Thus, the transformation of the given integral expressions, defined over the element Ω to one on the domain $\hat{\Omega}$ must be such as to facilitate numerical integration. Each element of the finite element mesh is transformed to $\hat{\Omega}$ only for the purpose of numerically evaluating the integrals. The element $\hat{\Omega}$ is called the master element. The geometric transformation from the physical element to master element can be done by linear mapping which is discussed below.

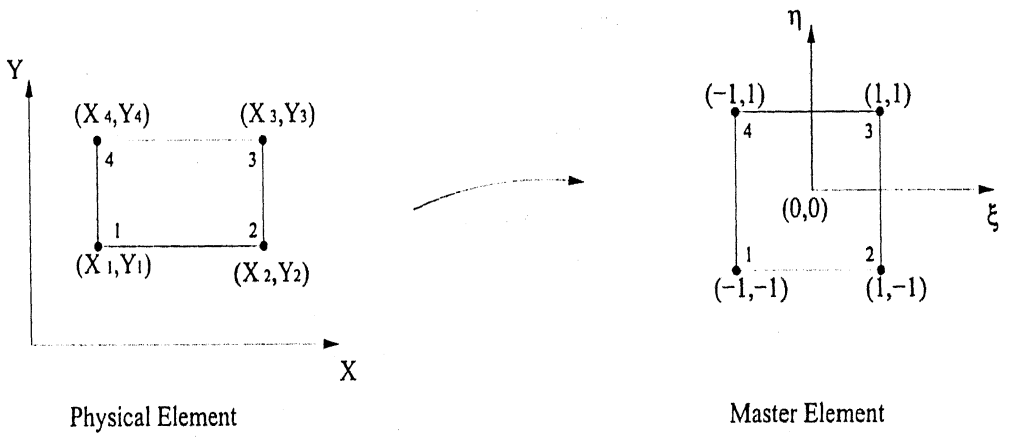

Figure 3.4: **Linear mapping in two dimensional domain**

The transformation between Ω^e and $\hat{\Omega}$ (or, equivalently between (x and y) and

(ξ and η) is accomplished by a coordinate transformation of the form

$$x(\xi,\eta) = \sum_{j=1}^{4}(X_j{}^e\,\hat{\psi}_j{}^e)\,;\;\; y(\xi,\eta) = \sum_{j=1}^{4}(Y_j{}^e\,\hat{\psi}_j{}^e) \tag{3.28}$$

where $X_j{}^e$ and $Y_j{}^e$ are the global coordinates on the physical element nodes and $\hat{\psi}_j{}^e$ denote the finite element interpolation functions of the master element $\hat{\Omega}$. Sub parametric formulation is used to represent geometry of the domain. Hence bilinear Lagrange interpolation functions are employed here.

$\hat{\psi_j}{}^e$ are defined in the following way.

$$\begin{aligned}
\hat{\psi_1}{}^e &= \frac{1}{4}(1-\xi)(1-\eta);\\
\hat{\psi_2}{}^e &= \frac{1}{4}(1+\xi)(1-\eta);\\
\hat{\psi_3}{}^e &= \frac{1}{4}(1+\xi)(1+\eta);\\
\hat{\psi_4}{}^e &= \frac{1}{4}(1-\xi)(1+\eta);
\end{aligned} \tag{3.29}$$

The transformation $\hat{\psi_i}{}^e$ can be expressed in terms of the local coordinates ξ and η by means of the. Hence by the chain rule of partial differentiation,we have

$$\begin{aligned}
\frac{\partial \psi_i{}^e}{\partial \xi} &= \frac{\partial \psi_i{}^e}{\partial x}\frac{\partial x}{\partial \xi} + \frac{\partial \psi_i{}^e}{\partial y}\frac{\partial y}{\partial \xi};\\
\frac{\partial \psi_i{}^e}{\partial \eta} &= \frac{\partial \psi_i{}^e}{\partial x}\frac{\partial x}{\partial \eta} + \frac{\partial \psi_i{}^e}{\partial y}\frac{\partial y}{\partial \eta}
\end{aligned} \tag{3.30}$$

which gives the relation between the derivatives of $\psi_i{}^e$ with respect to the global and local coordinates.

The matrix in the above equation is called the jacobian matrix of the transformation.

∎ *Transforming $dxdy$ into $d\xi d\eta$*

Let the differential area $dxdy$ is formed through vectors $\hat{dx}$ and $\hat{dy}$ with magnitude dA and direction normal to the elemental area is $\hat{K}$

$$dA = dx\,dy = [\,\hat{dx} \times \hat{dy}\,]\,.\,\hat{k} \tag{3.31}$$

$$\begin{aligned} dx\,dy &= [\,(\frac{\partial x}{\partial \xi}\,d\xi\,\hat{i} + (\frac{\partial x}{\partial \eta}\,d\eta\,\hat{j}\,) \times (\frac{\partial y}{\partial \xi}\,d\xi\,\hat{i} + \frac{\partial y}{\partial \eta}\,d\eta\,\hat{j}\,)\,] \\ &= [\frac{\partial x}{\partial \xi}\cdot\frac{\partial x}{\partial \eta} - \frac{\partial y}{\partial \xi}\cdot\frac{\partial y}{\partial \eta}\,]\,d\xi\,d\eta \\ &= |J\,|\,d\xi\,d\eta \end{aligned} \tag{3.32}$$

where

$$|J| = \frac{\partial x}{\partial \xi}\frac{\partial y}{\partial \eta} - \frac{\partial y}{\partial \xi}\frac{\partial x}{\partial \eta} \tag{3.33}$$

Hence $\int_e f\,(x,\,y)\,dx\,dy$ can be written as

$$\int_e f\,(x,\,y)\,dx\,dy = \int_{em} \hat{f}\,(\xi,\,\eta)\,d\xi\,d\eta \tag{3.34}$$

such that $\hat{f}\,(\xi,\,\eta) = |J|\,f\,(x\,(\xi,\,\eta),\,y(\xi,\,\eta)\,)$

The condition which must be satisfied for physically meaningful mapping of the domain is that,$|J| > 0$.

∎ *Numerical Integration*

Quadrature formula for integrals defined over the rectangular master element $\hat{\Omega}_R$ can be derived as follows.

$$\int_{\hat{\Omega}} \hat{f}\,(\xi,\,\eta)\,d\xi\,d\eta \approx \sum_{i=1}^{M}\sum_{j=1}^{N}\int_{\hat{\Omega}} \hat{f}\,(\xi_i,\,\eta_j)\,d\xi\,d\eta\;W_i\;W_j \tag{3.35}$$

where M and N denote the number of quadrature pints in the ξ and η directions, $(\xi_i,\,\eta_j)$ denote the Gauss points, and W_i and W_j denote the corresponding Gauss weights.Order of the numerical integration should be greater than or equal to $(p + 1)/2$ where, p is the order of the integrand.

In the present formulation 5×5 Gauss quadrature points have been used.

Chapter 4

Numerical Results and Discussion

4.1 Introduction

The present chapter deals with the validation and the various results obtained using the finite element formulation described in the previous chapter. The main aim is to study the initial buckling behaviour of laminated composite plates with and without cutouts, using a simple higher order shear deformation theory. For the present study it is assumed that there is no coupling between the in-plane and out-of-plane displacements, ie., symmetric lay-ups assumed. If this is not true, then even for an infinitesimally small in-plane compressive force the laminated composite plate will undergo flexure. For symmetric laminates this condition is automatically satisfied but for antisymmetric laminates there is always coupling between in-plane and out-of-plane quantities. In the case of antisymmetric laminates we have assumed that this coupling effect is negligibly small and was ignored to find the buckling load. This assumption although seems strong it can be shown that if the number of plies is increased the coupling effect dies out rapidly and the solution approaches the orthotropic solution (see [15]).

In the present study the following assumptions are made.

- The thickness of each layer is constant.
- There is no delamination/slip between the layers.

- No micro-buckling takes place before the initial buckling.
- There is no fibre breakage or matrix cracking before the onset of initial buckling.

In the current investigation the following nomenclatures are assumed to denote the thickness of laminate.

- $a/h \geq 100$: Thin laminate .
- $20 \leq a/h \leq 50$: Moderately thick laminate .
- $a/h \leq 10$: Very thick laminate .

This classification is tentative and actual definition depends on a variety of factors such as loadings, boundary conditions etc.

4.2 Boundary Conditions

The following types of geometric boundary conditions are considered in the numerical analysis.

- $u \neq 0$ and $v = 0$ along loaded edges ;
- $u = 0$ and $v \neq 0$ along unloaded edges ;
- Simply-Supported (S) : $w_b = w_s = 0$;
- Clamped (C) : $w_b = w_s = w_{b,n} = w_{s,n} = 0$;
  where, $n = x$ or y depending on the side of the plate.

To define the complete set of boundary conditions on all four sides of the plate the following scheme has been adopted which is explained through an example.

SCCS denotes the following set of boundary contitions:

$$w_b = w_s = 0 \qquad at\ x = 0\ \forall\ y$$
$$w_b = w_s = w_{b,y} = w_{s,y} = 0 \qquad at\ y = 0\ \forall\ x$$
$$w_b = w_s = w_{b,x} = w_{s,x} = 0 \qquad at\ x = a\ \forall\ y$$
$$w_b = w_s = 0 \qquad at\ y = b\ \forall\ x$$

4.3 Material Properties

Computations were carried out for the following material properties.

Table 4.1: **Material properties**

Material code	$E_L(GPa)$	$\frac{E_L}{E_T}$	$\frac{G_{LT}}{E_T}$	$\frac{G_{LT'}}{E_T}$	$\frac{G_{TT'}}{E_T}$	ν_{LT}
M1 [7]*	130	13	0.5	0.5	0.2	0.35
M2 [12]*	200	40	0.6	0.6	0.5	0.25
M3	100	isotropic				0.25
M3 [7]*	153	15.904	0.616	0.616	0.336	0.32

*Numbers in the brackets represents the references given in the bibilograply.

4.4 Convergence Study

In this section, the convergence study of the laminated composite plates without cutouts is discussed.

Convergence of the initial buckling load with mesh refinement is as shown in Table 4.2. Here for all cases Material Code = M1, Aspect Ratio = 1.0 and length/thickness ratio = 10.

From Table 4.2 it can be concluded that for a square plate, a 10×10 mesh gives sufficiently accurate results (for both simply supported and clamped boundary conditions) from engineering point of view.

For rectangular plates, it has been observed that for $a/b = 2$ sufficiently converged result can be obtained with a 10×5 mesh whereas for $a/b = 3$ a 15×5, mesh is sufficient for both simply supported and clamped boundary conditions.

Table 4.2: **Convergence study**

Boundary condition	Laminate lay-up sequence	Mesh size	Nondimensionalized buckling load, N_x ($\bar{N}_x = N_x b^2/E_t h^3$)
SSSS	$[90/0]_s$	2×2	7.4943
		4×4	9.3565
		8×8	9.4372
		10×10	9.4441
CCCC	$[90/0]_s$	2×2	12.6457
		4×4	15.3898
		8×8	15.9465
		10×10	16.0501
SSSS	$[90/0/90/0]_2$	2×2	10.3057
		4×4	10.9218
		8×8	11.0400
		10×10	11.0477
SCCS	$[90/0/90/0]_2$	2×2	24.2386
		4×4	27.1568
		8×8	27.9157
		10×10	27.9212

4.5 Validation Study

The validation of the finite element plate model is accomplished by comparing the results of the following set of problems with results published in the literature. Here for all cases material code = M2, aspect ratio = 1.0, boundary condition = SSSS and laminate lay-up sequence = $[0/90]_5$. The validation study is made for the problems defined in Table 4.3.

The comparative study of the analytical results from the present investigation with the results available in the published literature is presented in Table 4.4.

Table 4.3: **Problem definitions for validation study**

Problem number	Material code	Aspect (a/b)	Thickness ratio(a/h)	Boundary conditions	laminae lay-up sequence
P13	M3	1.0	100	SSSS	isotropic
P14	M3	1.0	100	CCCC	isotropic
P15	M2	1.0	10	SSSS	$[0/90]_5$
P16	M2	1.0	10	SSCS	$[0/90]_5$
P17	M2	1.0	10	CSCS	$[0/90]_5$
P18	M2	1.0	5	SSSS	$[0/90]_5$
P19	M2	1.0	5	SSCS	$[0/90]_5$
P20	M2	1.0	5	CSCS	$[0/90]_5$

From Table 4.4 can be observed that the difference in the results obtained from the present study and those of Ref.[12] is less than 2.5% in all the cases. Hence we can conclude that the present formulation gives reasonable results and has been validated.

Table 4.4: **Validation study**

Thickness ratio(a/h)	Laminate theory [ref. no.]	Reference		Present	
		N_x	N_y	N_x	N_y
P13	CLT [16]	4.0	-	3.997	-
	HSDT	-	-	-	-
P14	CLT [16]	10.15	-	10.032	-
	HSDT	-	-	-	-
P10	CLT [12]	35.232	35.232	36.198	36.198
	HSDT [12]	25.828	25.828	25.943	25.943
P16	CLT [12]	-	59.288[a]	-	60.563[c]
	HSDT [12]	-	33.662[b]	-	33.969
P17	CLT [12]	-	89.770[a]	-	91.015[c]
	HSDT [12]	-	36.657[b]	-	35.958
P5	CLT [12]	-	35.232	-	36.198
	HSDT [12]	-	12.224	-	12.603
P19	CLT [12]	-	59.288[a]	-	60.563[c]
	HSDT [12]	-	12.800[b]	-	12.969
P20	CLT [12]	-	89.770[a]	-	91.015[c]
	HSDT [12]	-	13.659[b]	-	13.426

[a] Results obtained with the exact solution developed in the corresponding reference.

[b] Results using the finite element solution in the corresponding reference.

[c] Results obtained by supressing w_s over the entire domain of the plate.

$\bar{N}_x/\bar{N}_y$ are the dimensionless initial buckling values where the nondimensionalizing factor is as given in the corresponding references.

4.6 Prebuckling Analysis

The buckling analysis of plates with cutout necessiates the need for inplane stress distribution in the plate as it is no longer uniform which is not the case with a plate which is continous. Due to possibility of steep stress gradients being present the use of a variable mesh spacing is necessary, as it is well known that the success of any method for the determination of critical loads is dependent on the accuracy of the plane stress distrubution being used.

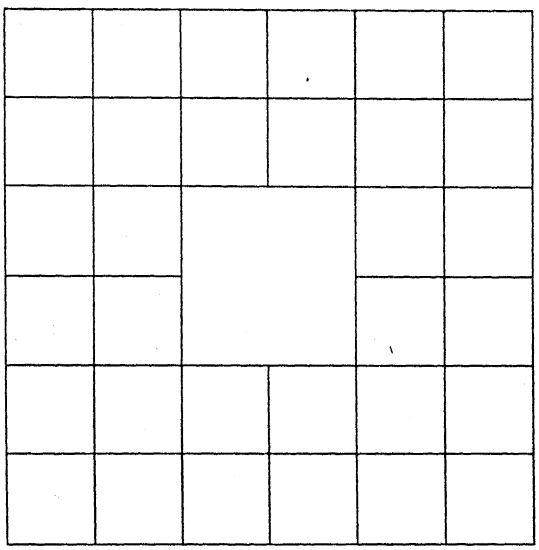

Figure 4.1: **Equal mesh**

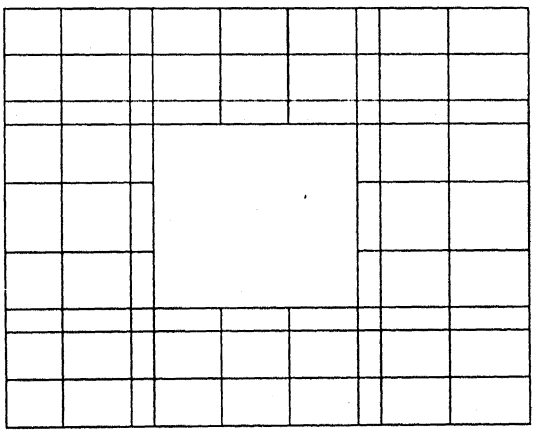

Figure 4.2: **Graded mesh**

The in-plane stress resultants are calculated in conventional manner from the original displacement functions used in deriving the stiffness of the element. The in-plane stress resultants are calculated at the centre of each finite element and these are further used in the formation of the geometric stiffness matrix. Two different meshes, the equal and the graded mesh, are employed to study the in-plane stress distrubution and also the flexure analysis.Figures 4.1 and 4.2 shows the equal and graded meshes. The mesh around the cutout is refined in a graded mesh to capture the stress gradients near the cutout corners. Figures 4.3 and 4.4 clearly shows the in-plane stress distribution in a plate at a given section x-x. From the figures it has been observed that the graded mesh gives good results compared to equal mesh.

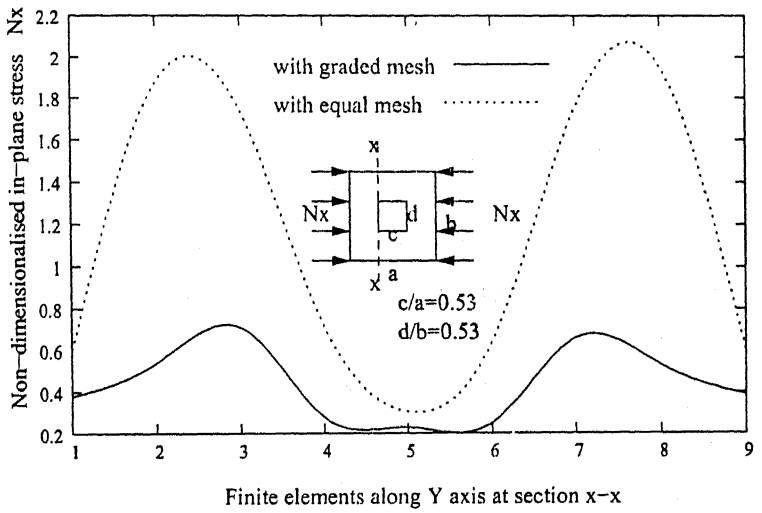

Figure 4.3: **In-plane stress vs Correspondng finite element in Y direction**

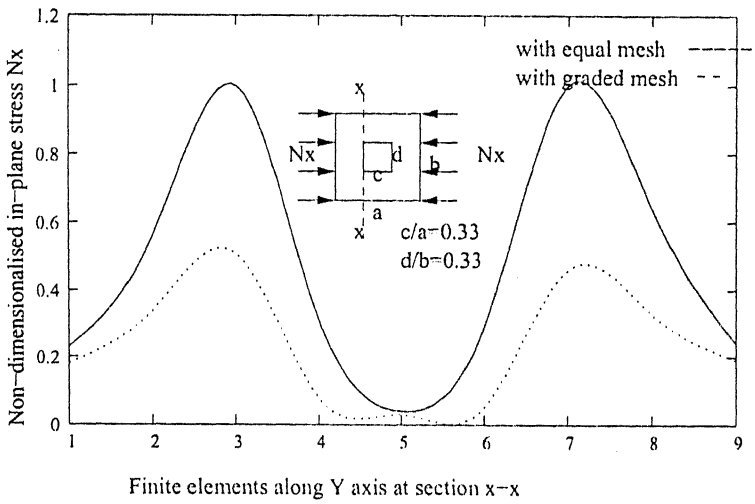

Figure 4.4: **In-plane stress vs Correspondng finite element in Y direction**

4.7 Validation of Plate Model With Cutout

The results for an isotropic laminate with cutout is compared with the results given in [8]. Figure 4.5 shows the plot of buckling load for an isotropic laminate with varying hole ratio with all edges simply supported. From the plot it can be seen that the present method gives reasonably good result.Thus a 9×9 mesh gives sufficiently accurate result for the plate with cutout. It is observed that the buckling load decreases continuously with the increase in hole size. For both the finite element models the results are very close for small hole size. However the discrepancy is observed to be more for larger hole sizes. It is difficult to comment on the finite element model in the absence of closed form solution.

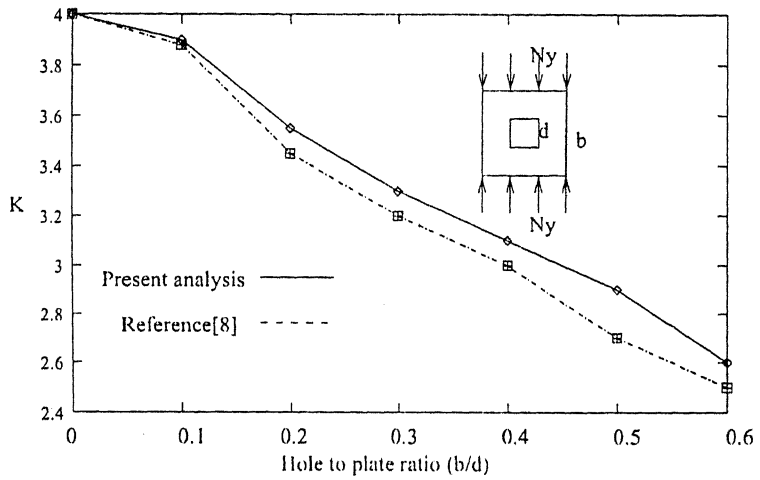

Figure 4.5: **Buckling load vs Plate to hole ratio Y-direction under in-plane load N_y , (Isotropic Material), a/b=1**

4.8 Parametric Study of Composite Laminates With and Without Cutout

In this section the effects of plate aspect ratio (a/b), length/thickness ratio (a/h) and fibre orientation angle (θ) on the initial buckling load of laminated (8 layer antisymmetric, $[\pm\theta]_4$ composite plate, with and without a cutout, is studied (using HSDT) keeping the material properties constant (Material - M2) under uniaxial in-plane compressive loadings. The geometric boundary conditions considered are simply supported on all sides.

The results are presented for the composite laminates with and without a cutout. It can be seen from the Figs.4.6-4.9 that for a thin laminate $(a/h = 100)$ the fibre orientation angle for the maximum value of the fundamental initial buckling load (henceforth the fibre orientation angle for the maximum value of the fundamental initial buckling load is denoted as $(\theta_{cric.})$ and the corresponding initial buckling load as the critical buckling load) is around 45° for aspect ratio's $(a/b = 1, 2, 3)$. The cricical buckling load decreases very slightly with the increase in aspect ratio.

With increase in the thickness of the laminate transverse shear plays a dominant role in the buckling behaviour of the laminate. For $a/h = 50$ the fibre orientation

angles for critical initial buckling load are about 45°, 42° and 40° respectively, for aspect ratio's $a/b = 1, 2, 3$.

As the laminate becomes thicker there is a shift in the cricital fiber orientation angle towards lesser values. Also this shift is more as the aspect ratio increases. For thick laminate ($a/h = 10$) the effect of fibre orientation angle on the value of critical buckling load decreases with the increase in aspect ratio. The decrease in the values of initial buckling load is more pronounced for thick laminates. This brings out the fact that for thick laminates one should consider transverse shear effects.

The results presented in Figs. 4.10 - 4.12 show the effect of a centrally located cutout on the behaviour of critical buckling load. It can be seen that the critical fibre orientation angle ($\theta_{cric.}$) is still 45° for a thin laminate ($a/h = 100$) for aspect ratio ($a/b = 1$). But for aspect ratio's ($a/b = 2, 3$) the critical fibre orientation angle is 52° and 55° and there is a shift of 10 degrees, as a/b ratio increases from 1 to 3.

Figs. 4.12-4.20 shows the variation of buckling load with and without cutout for aspect ratio's ($a/b = 1, 2, 3$). From Figs. 4.12-4.20 we could observe that for aspect ratio $a/b = 1$, the critical buckling load of the plate with a cutout approaches that of a plate without a cutout for orientation angles 65° to 90°. But this trend is not observed for the aspect ratio's 2 and 3. The shift in the cricital fibre orientation angles is clearly shown in the Figs. 4.12- 4.20. Also it can be seen that the plots are no longer symmetric for plates with a cutout

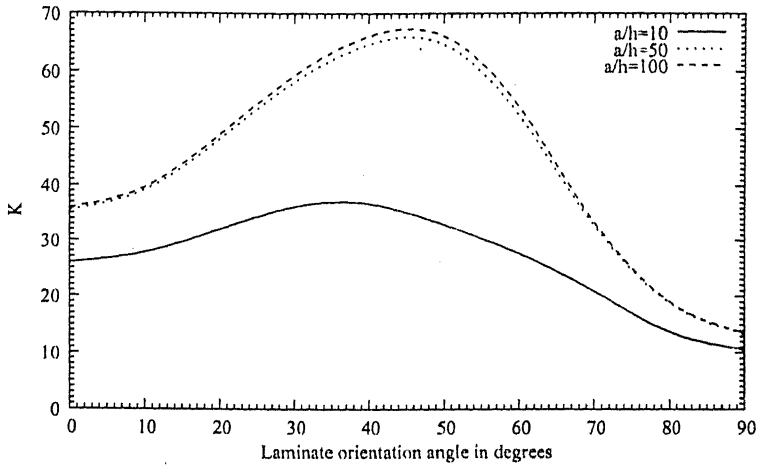

Figure 4.6: **Non-dimensionalized initial buckling load versus fibre orientation (θ), (Material- M2), a/b=1.**

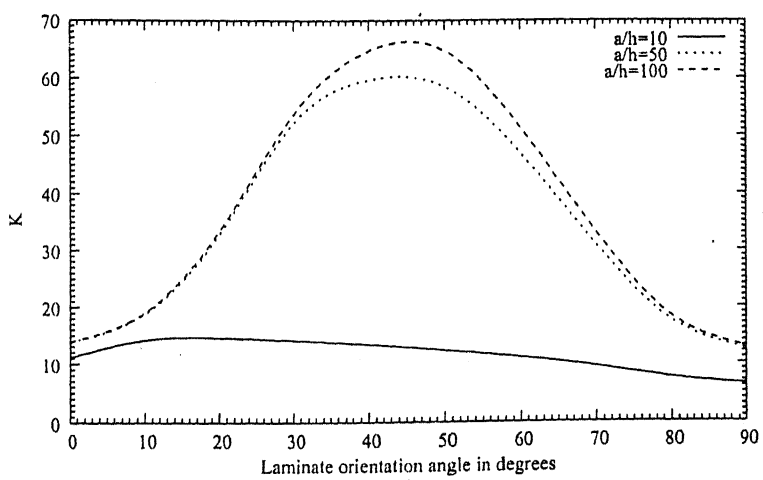

Figure 4.7: **Non-dimensionalized initial buckling load versus fibre orientation (θ), (Material- M2), a/b=2.**

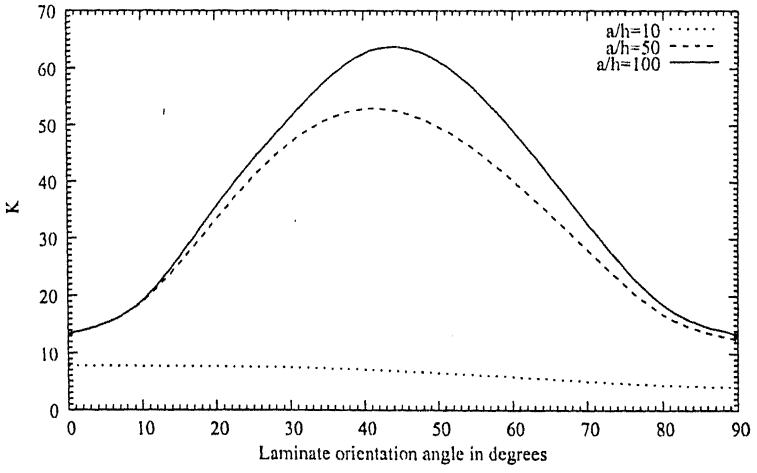

Figure 4.8: **Non-dimensionalized initial buckling load versus fibre orientation (θ), (Material- M2), a/b=3.**

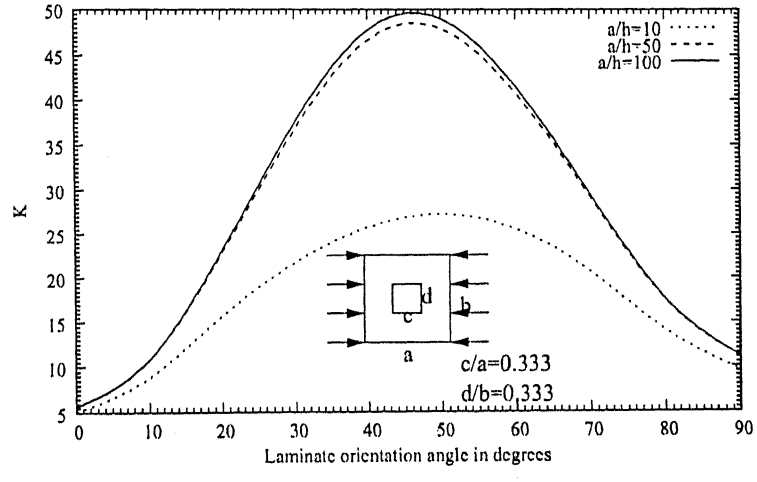

Figure 4.9: **Non-dimensionalized initial buckling load versus fibre orientation (θ) with a cutout , (Material- M2), a/b=1.**

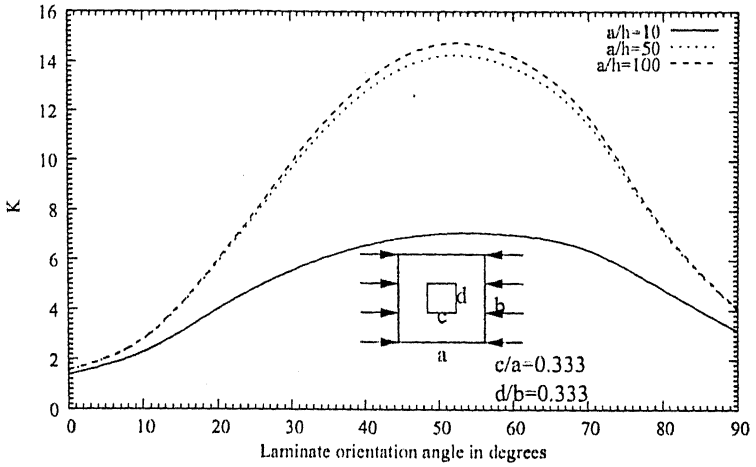

Figure 4.10: **Non-dimensionalized initial buckling load versus fibre orientation (θ) with a cutout , (Material- M2), a/b=2.**

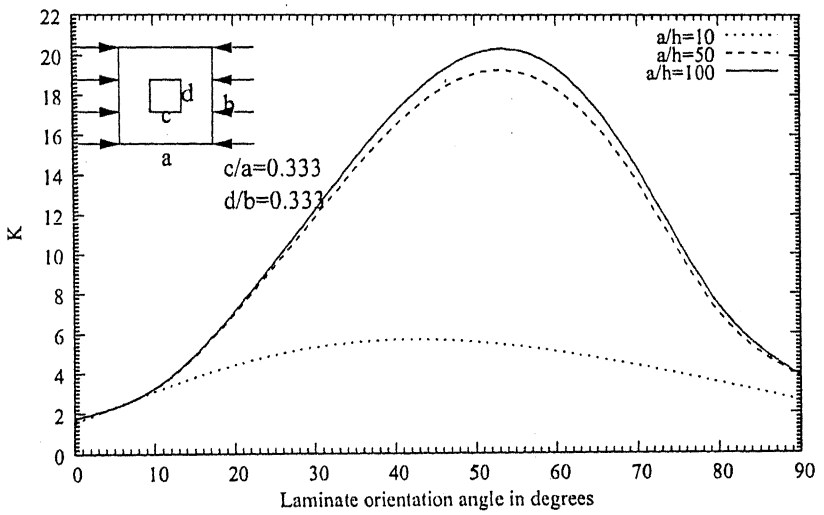

Figure 4.11: **Non-dimensionalized initial buckling load versus fibre orientation (θ) with a cutout , (Material- M2), a/b=3.**

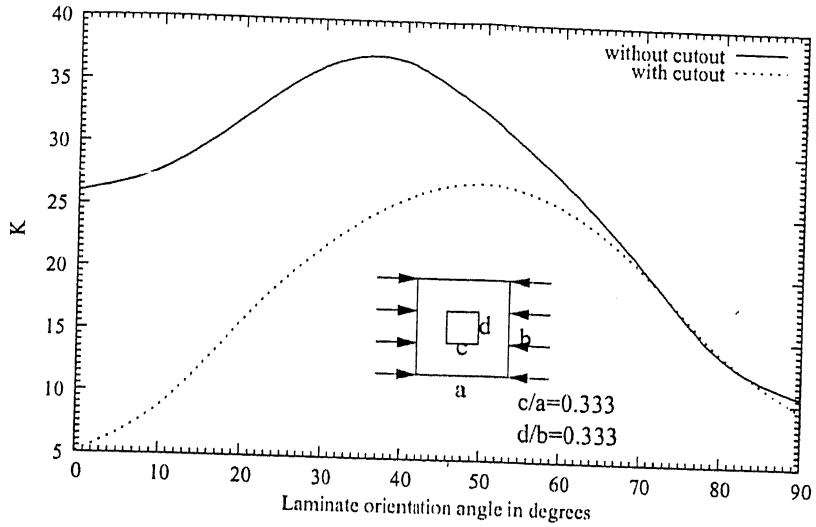

Figure 4.12: Non-dimensionalized initial buckling load versus fibre orientation (θ) with and without cutout , (Material- M2), a/b=1, a/h=10.

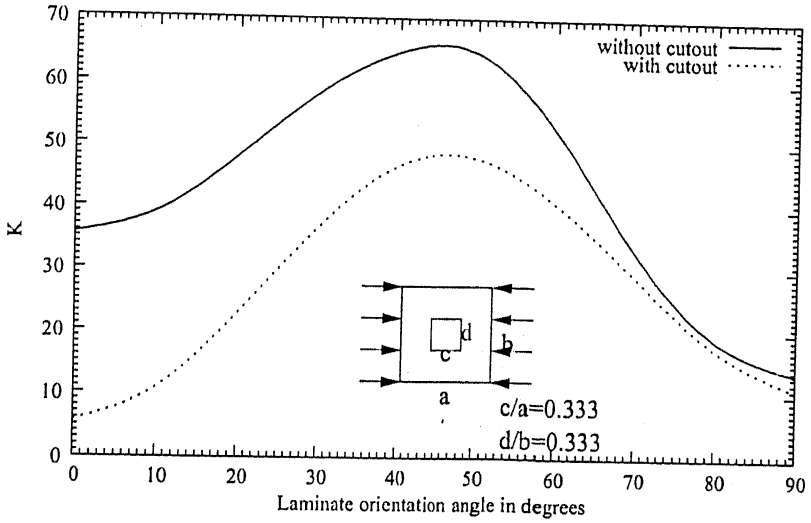

Figure 4.13: Non-dimensionalized initial buckling load versus fibre orientation (θ) with and without cutout , (Material- M2), a/b=1, a/h=50.

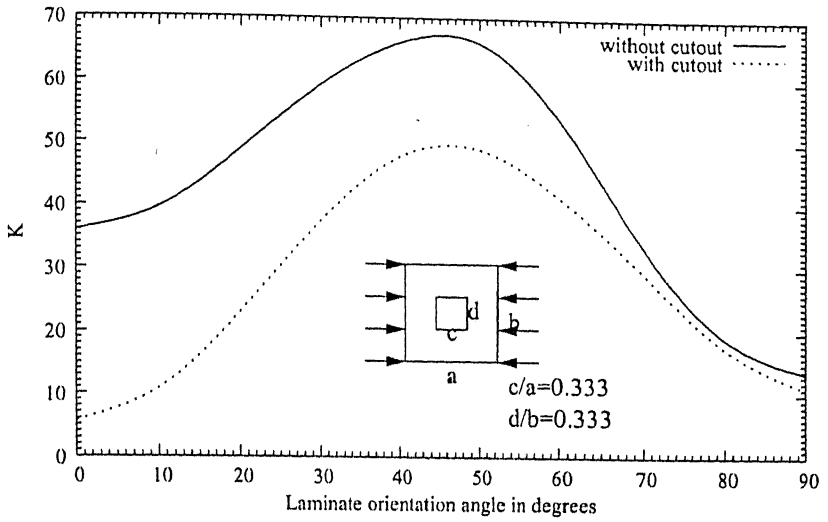

Figure 4.14: **Non-dimensionalized initial buckling load versus fibre orientation (θ) with and without cutout. , (Material- M2), a/b=1, a/h=100.**

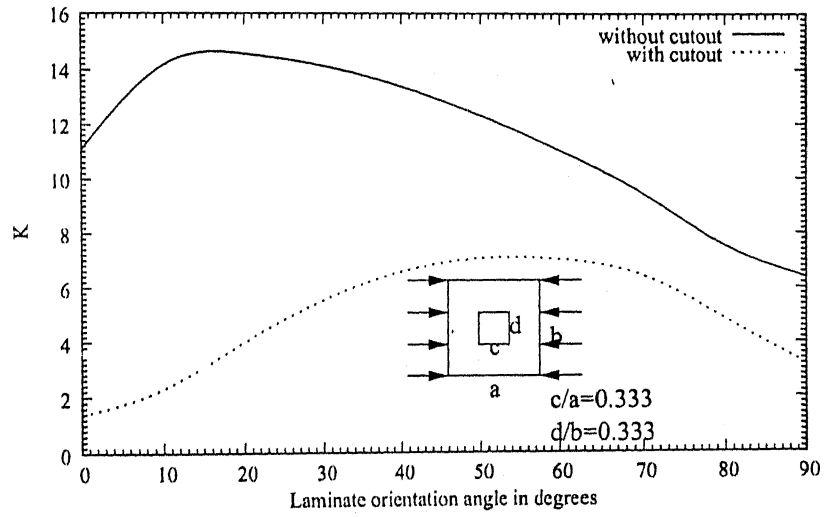

Figure 4.15: **Non-dimensionalized initial buckling load versus fibre orientation (θ) with and without cutout , (Material- M2), a/b=2, a/h=10.**

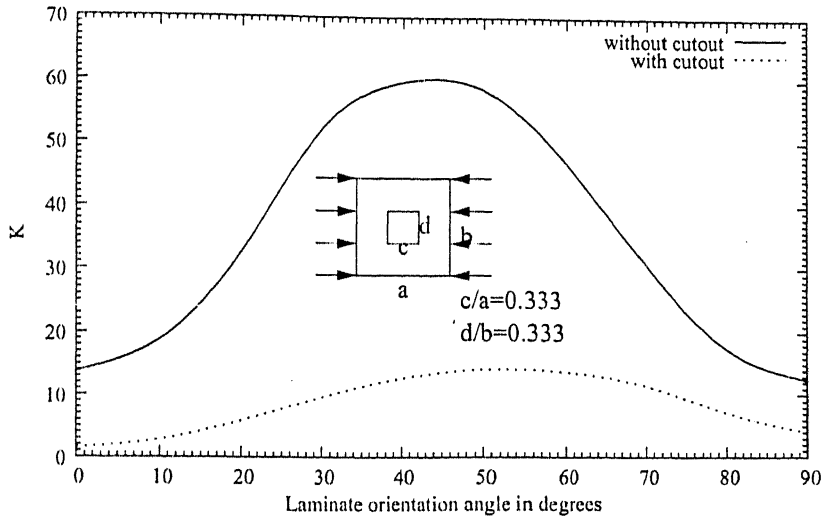

Figure 4.16: Non-dimensionalized initial buckling load versus fibre orientation (θ) with and without cutout , (Material- M2), a/b=2, a/h=50.

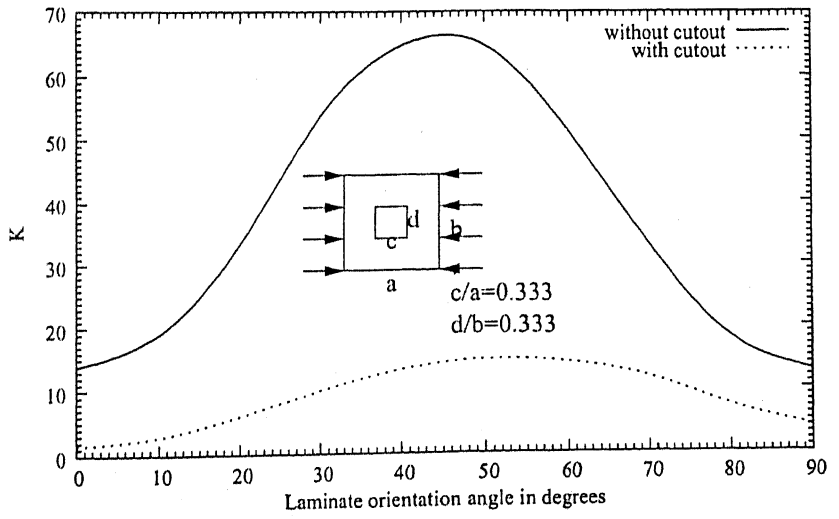

Figure 4.17: Non-dimensionalized initial buckling load versus fibre orientation (θ) with and without cutout. , (Material- M2), a/b=2, a/h=100.

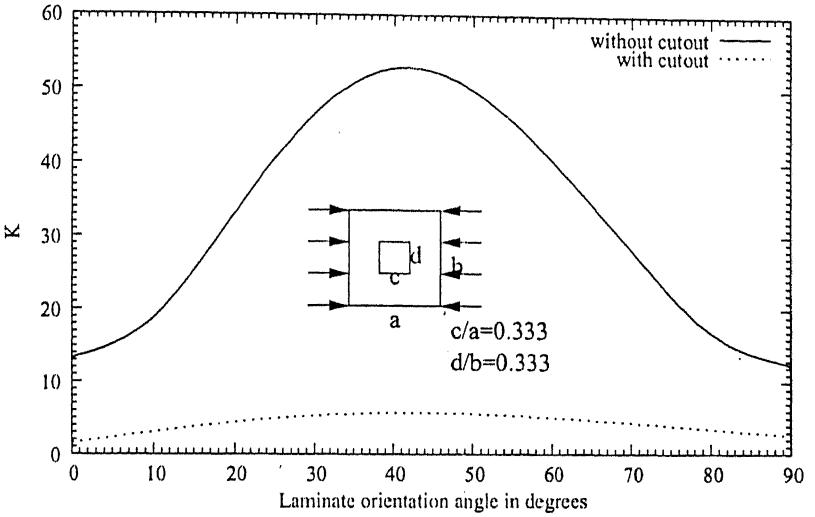

Figure 4.18: **Non-dimensionalized initial buckling load versus fibre orientation (θ) with and without cutout , (Material- M2), a/b=3, a/h=10.**

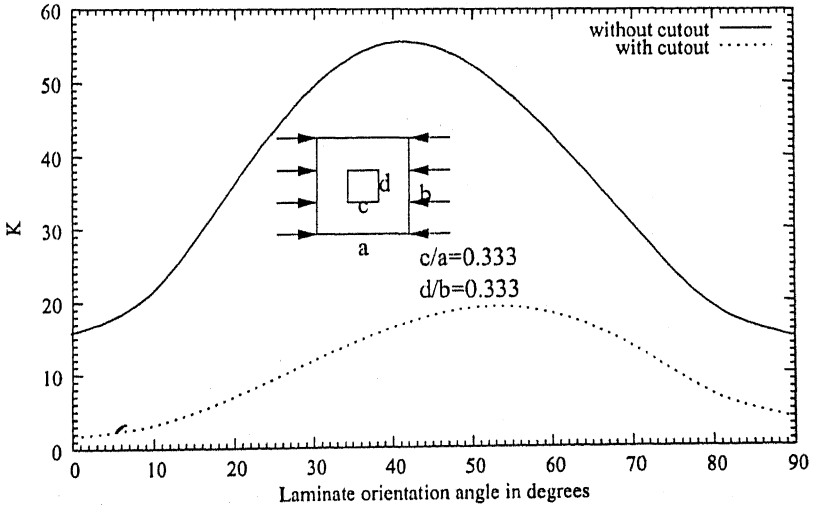

Figure 4.19: **Non-dimensionalized initial buckling load versus fibre orientation (θ) with and without cutout , (Material- M2), a/b=3, a/h=50.**

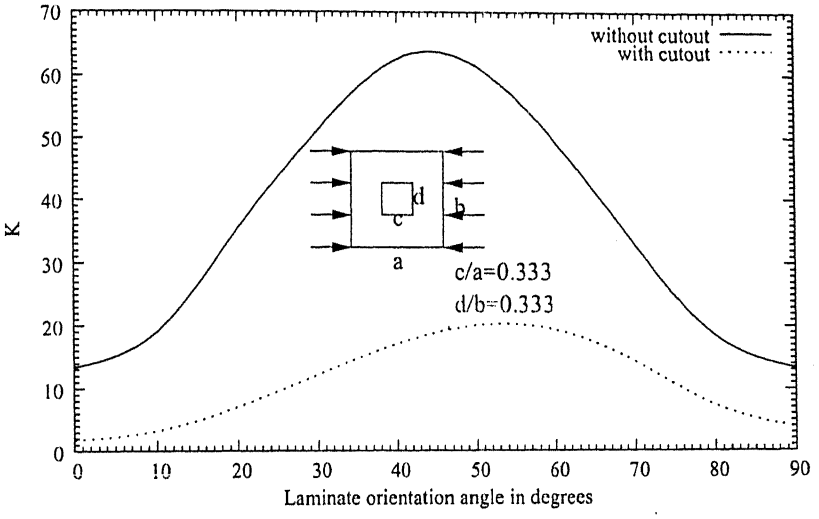

Figure 4.20: **Non-dimensionalized initial buckling load versus fibre orientation (θ) with and without cutout. , (Material- M2), a/b=3, a/h=100.**

4.9 Biaxial In-Plane Loadings N_x and N_y

This section deals with the study of stability envelops under biaxial loading on the response of laminated composite plate with and without a cutout. The results for a plate without a cutout are compared with the results available in the literature. [13]. It is found that the results are in very good agreement with the results in the literature.

Figs. 4.21-4.28 show the stability envelops under biaxial loadings for plate aspect ratio's ($a/b = 1, 2$) and length/thickness ratio's 10 and 100. K_x in the figures represent the nondimensionalised buckling load ($K_x = N_x b^2/E_t h^3$) and ($K_y = N_y b^2/E_t h^3$).

For $a/b = 1$ and $a/h = 10$. Figs. 4.21 and 4.25 show the interaction curves without a cutout and with a cutout. The following observations can be made from the figures.

- Except for cross ply laminates the stability envelops for all angle ply laminates are linear for a plate without a cutout. But this behaviour is not observed for the case of a plate with a cutout.
- $\theta = 45°$ gives the highest value of (N_x and N_y) for any combination of the loads

in both the cases and for cross ply laminate (N_x and N_y) is the mininum.

- There is a sudden change in the slope of stability envelops for almost all laminates for a plate with a cutout. Whereas when it comes to plate without a cutout, there is no such sudden change of slope .

- From the stablity envelops shown in Fig. 4.21, it can be observed that for $\theta = 30°$ and $\theta = 60°$ laminates there is a region between two points in which both the laminates have the same interaction curve. But when it comes to a plate with a cutout, $\theta = 30°$ and $\theta = 45°$ laminates has the same interaction curve at a single point. At this particular point, both these laminates withstand the same amount of buckling load.

Figs. 4.22 and 4.26 show the interaction curves for a plate without a cutout and with a cutout. The following are the observations that can be made from the figures.

- The stability envelops are linear or piece wise linear for a plate without a cutout whereas they are no longer linear for a plate with a cutout.

- $\theta = 45°$ gives the highest value of (N_x and N_y) for any combination of the loads in both the cases and for cross ply laminate ($N_x and N_y$) is the mininum.

- There is a sudden change in the slope of stability envelops for almost all laminates for a plate with a cutout. Whereas when it comes to plate without a cutout, the slope changes only for $\theta = 30°$ and $\theta = 60°$ laminate.

- The portion for which $(N_x + N_y)$ is same for both $\theta = 30°$ and $\theta = 60°$ laminates is less as compared to thin laminates.

- Comparing the magnitude of the buckling loads for plate with and without cutout, we can observe that there is some 40 precentage reduction in the buckling load.

For $a/b = 2$ and $a/h = 10$ (Fig.4.23 and Fig. 4.27) the following observations are made.

- Here for both the cases ie.,plate without a cutout and with a cutout, the stability envelops are piecewise linear but for certain portions of the envelops there is a change in the slope.

- The curves are almost perpendicular to the Y axis for one portion of them and are almost perpendicular to the X axis for the other portion. This is due to the fact that at these portions of the curves, for a small decrease in the value of N_x the strength of the laminate to carry N_y increases rapidly.

- From Fig. 4.22 we can observe that $\theta = 45°$ and $\theta = 60°$ laminates have interaction curve at one particular point. There is a reduction in the buckling load when it comes for a plate with a cutout.

For $a/b = 2$ and $a/h = 100$ (Fig.4.24 and Fig. 4.28) the following observations are made.

- Here for both the cases ie., plate without a cutout and with a cutout, the stability envelops are piecewise linear.

- For different combinations of N_x and N_y , either $\theta = 45°$ or $\theta = 60°$ laminate gives the maximum value of $(N_x + N_y)$.

- For crossply laminate, the slope of the stability envelop changes at high value of N_y for both the cases, ie., for plate without and with a cutout, for $\theta = 45°$ laminate change in slope occurs at high value of N_x whereas $\theta = 60°$ laminate, change in slope occurs twice. One is when both N_x and N_y are high and another is when only N_x is high and N_y is small.

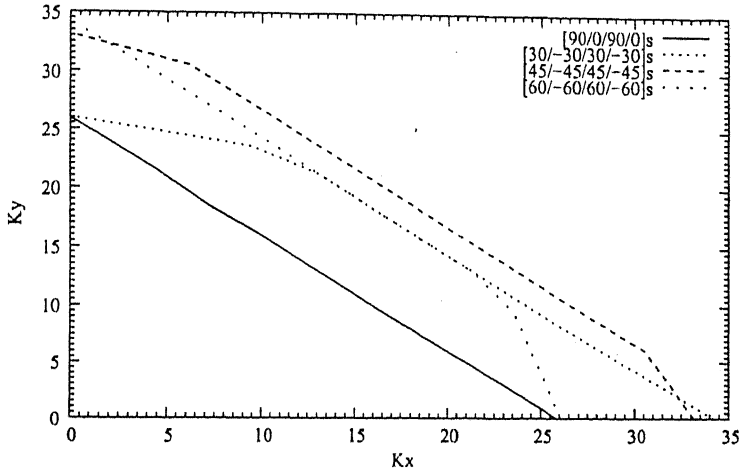

Figure 4.21: **Comparative study of stability envelop for biaxial in-plane compressive loads N_x and N_y, (Material- M2), a/b=1, a/h=10, without cutout, ($b = 254mm, h = 2.112mm$).**

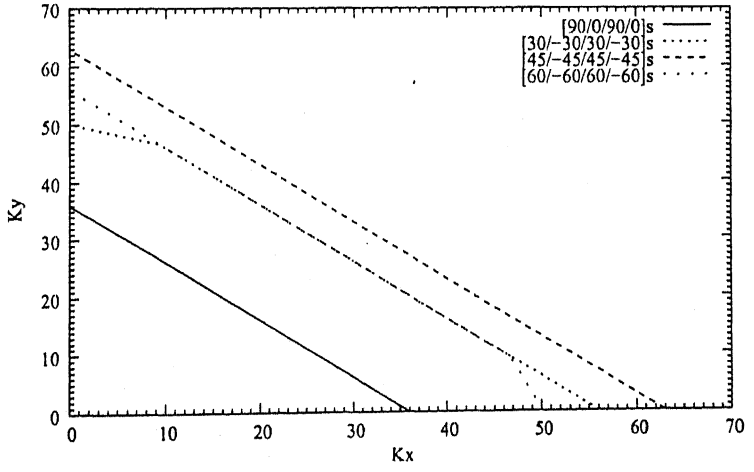

Figure 4.22: **Comparative study of stability envelop for biaxial in-plane compressive loads N_x and N_y, (Material- M2), a/b=1, a/h=100, without cutout, ($b = 254mm, h = 2.112mm$).**

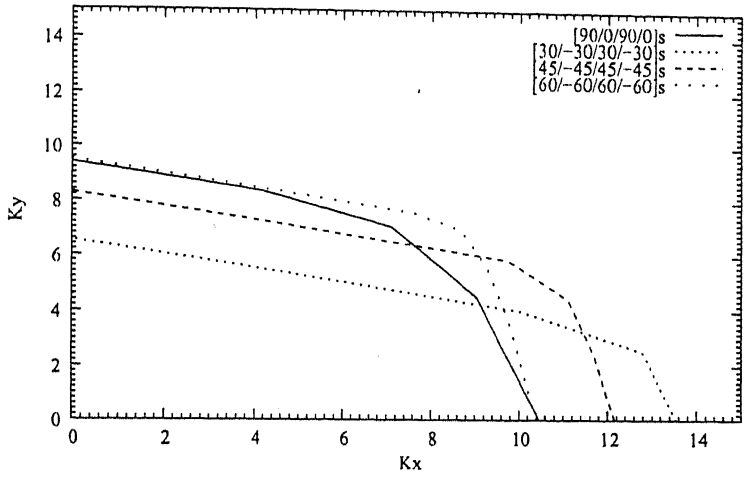

Figure 4.23: **Comparative study of stability envelop for biaxial in-plane compressive loads N_x and N_y, (Material- M2), a/b=2, a/h=10, without cutout, ($b = 254mm, h = 2.112mm$).**

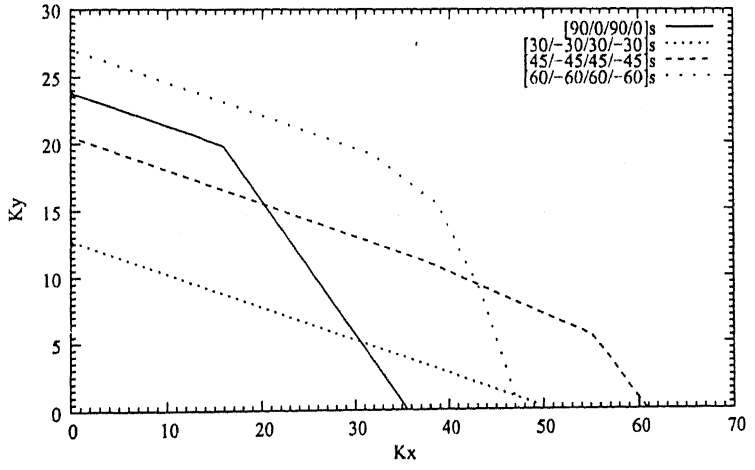

Figure 4.24: **Comparative study of stability envelop for biaxial in-plane compressive loads N_x and N_y, (Material- M2), a/b=2, a/h=100, without cutout, ($b = 254mm, h = 2.112mm$).**

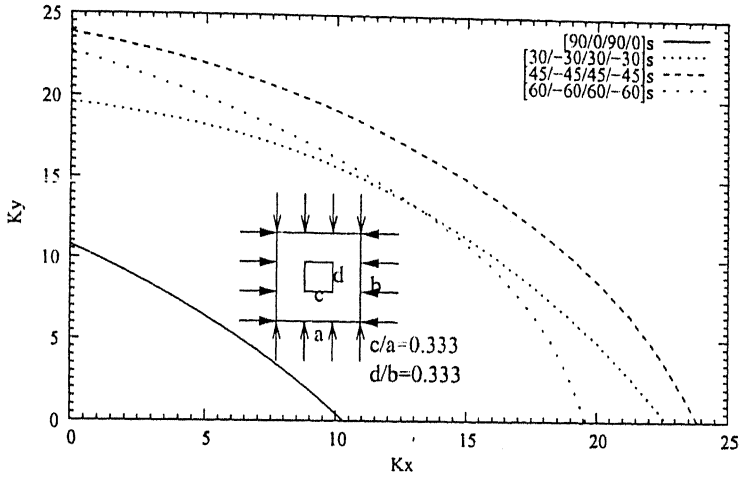

Figure 4.25: **Comparative study of stability envelop for biaxial in-plane compressive loads N_x and N_y, (Material- M2), a/b=1, a/h=10, with cutout,** $(b = 254mm, h = 2.112mm)$.

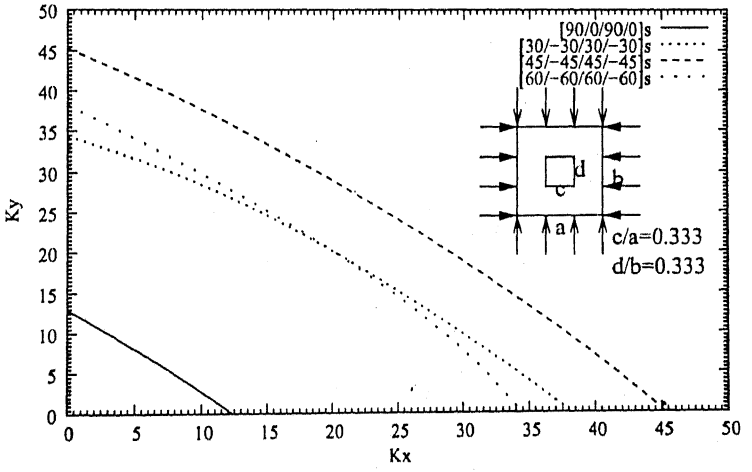

Figure 4.26: **Comparative study of stability envelop for biaxial in-plane compressive loads N_x and N_y, (Material- M2), a/b=1, a/h=100, with cutout,** $(b = 254mm, h = 2.112mm)$.

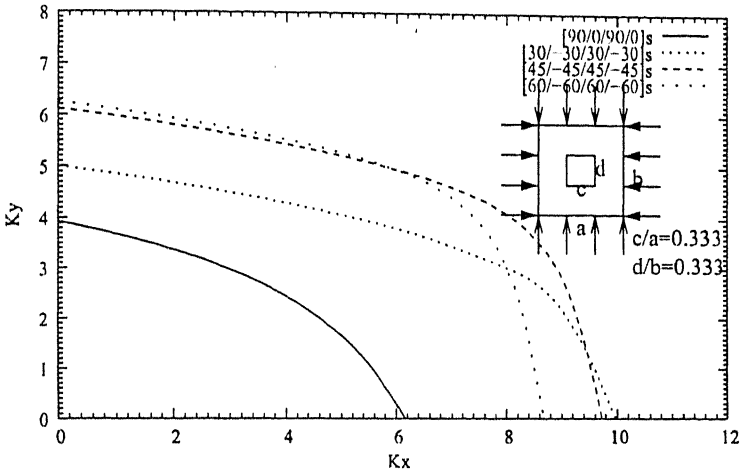

Figure 4.27: **Comparative study of stability envelop for biaxial in-plane compressive loads N_x and N_y, (Material- M2), a/b=2, a/h=10, with cutout,** $(b = 254mm, h = 2.112mm)$.

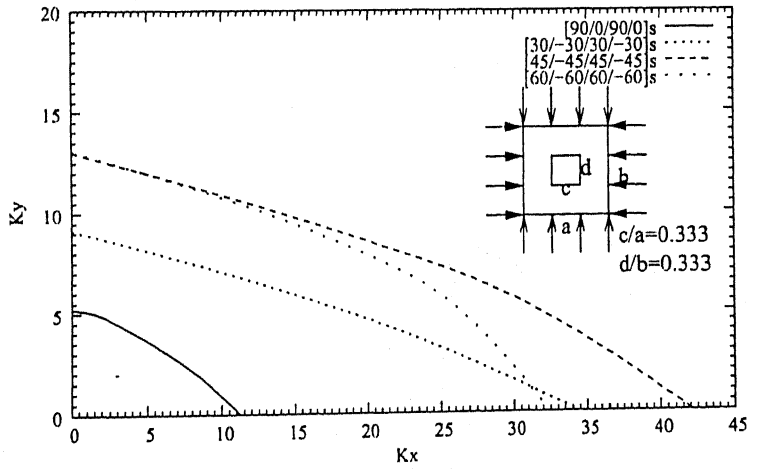

Figure 4.28: **Comparative study of stability envelop for biaxial in-plane compressive loads N_x and N_y, (Material- M2), a/b=2, a/h=100, with cutout,** $(b = 254mm, h = 2.112mm)$.

4.10 Biaxial In-Plane Loadings N_x and N_{xy}

In this section stabily envelops are shown for both crossply and angleply symmetric laminates $[\pm\theta]_{2S}$ with plate aspect ratio's 1 and 2 and length/thickness ratio's 100 and 10 for both square and rectangular laminates. Figures 4.29 -4.39 shows the interaction curves for N_x and N_{xy}

For a/b=1 and a/h=100 (Figs. 4.29 and 4.31) the following observations are made.

- Stability envelops are not symmetric about $N_{xy} = 0$ line except for a crossply laminate for both the cases, ie.,with and without a cutout. It is observed that the value of $(N_x + |N_{xy}|)$ for initial buckling load is more for positive shear as comapared to negative shear. This trend is also observed in the plate with a cutout.

- Stability envelops $\theta = 30°$ and $\theta = 60°$ laminates are comparable though $\theta = 30°$ laminate gives slightly higher values of $(N_x + |N_{xy}|)$.

- From the figures we could observe that there is no such unique point at which two or more laminates carry the same amout of axial compressive and shear loads.

For a/b=1 and a/h=100 (Figs. 4.30 and 4.32) the following observations are made.

- Stability envelops are not symmetric about $N_{xy} = 0$ line except for a crossply laminate for both the cases, ie.,with and without a cutout. It is observed that the value of $(N_x + |N_{xy}|)$ for initial buckling is more for positive shear as comapared to negative shear. This trend is also observed in the plate with a cutout.

- For negative shear loading the stability envelops of $\theta = 30°$ and $\theta = 45°$ laminates are comparable with each other while $\theta = 60°$ and crossply laminates are comparable with each other. The same trend can be observed in a plate with a cutout.

- For both the cases the interaction curves for the laminates intersect each others at some unique points. At these points different laminates carry the same amount of biaxial loads, N_x and N_{xy}. In other words it can be said that there are some unique combinations of in-plane compressive and shear loadings that can be carried out by different laminates.

- From the figures we could observe that there is a reduction in the buckling load in all the laminates when a cutout is placed in the plate. The variation varies for different laminates.

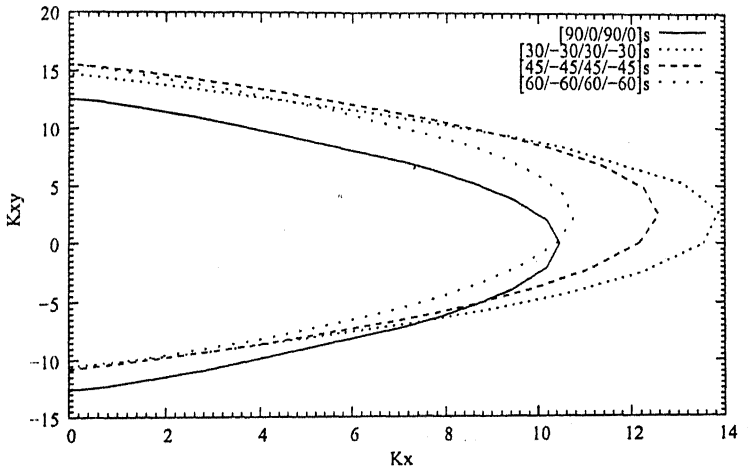

Figure 4.29: **Comparative study of stability envelop for biaxial in-plane compressive and shear loads N_x and N_{xy}, (Material- M2), a/b=1, a/h=10, without cutout, ($b = 254mm, h = 2.112mm$).**

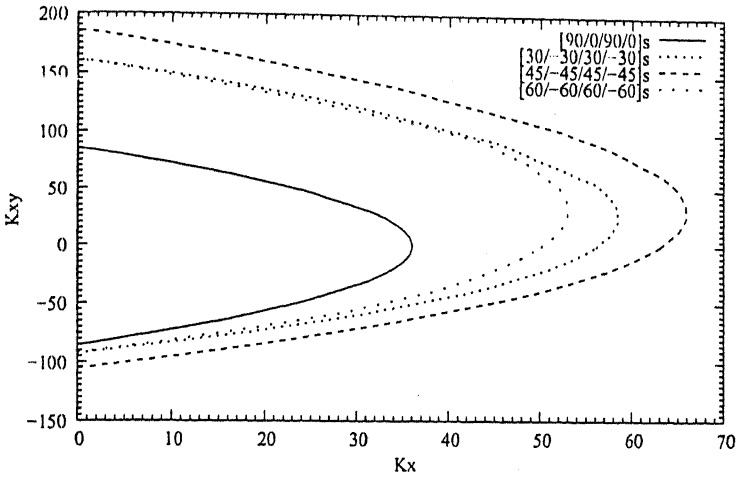

Figure 4.30: **Comparative study of stability envelop for biaxial in-plane compressive and shear loads N_x and N_{xy}, (Material- M2), a/b=1, a/h=100, without cutout, ($b = 254mm, h = 2.112mm$).**

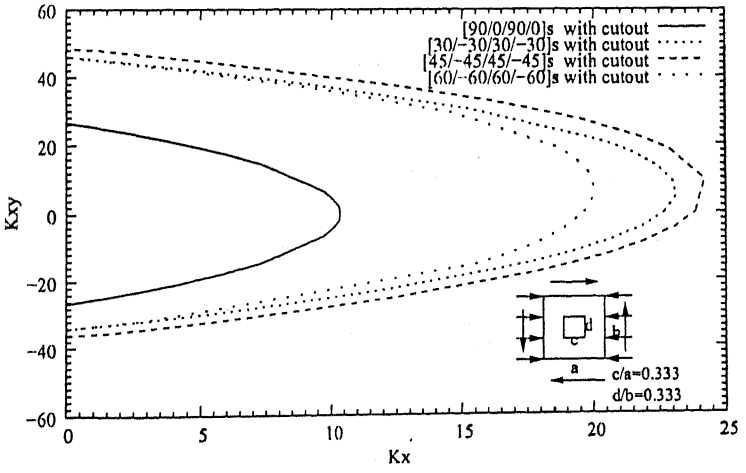

Figure 4.31: **Comparative study of stability envelop for biaxial in-plane compressive and shear loads N_x and N_{xy}, (Material- M2), a/b=1, a/h=10, with cutout, ($b = 254mm, h = 2.112mm$).**

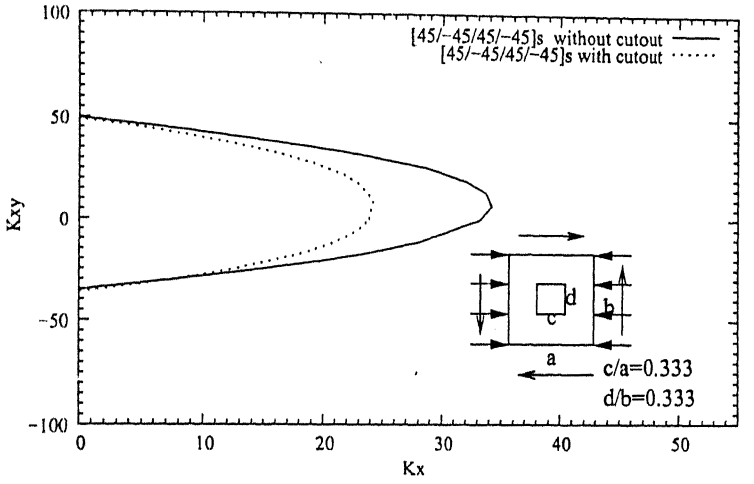

Figure 4.34: **Comparative study of stability envelop for biaxial in-plane compressive and shear loads N_x and N_{xy} with and without cutout, (Material- M2), a/b=1 a/h=10, ($b = 254mm, h = 2.112mm$).**

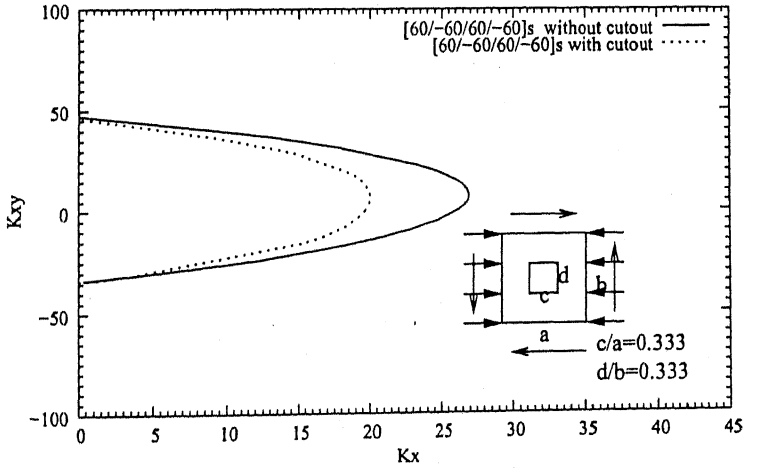

Figure 4.35: **Comparative study of stability envelop for biaxial in-plane compressive and shear loads N_x and N_{xy} with and without cutout, (Material- M2), a/b=1 a/h=10, ($b = 254mm, h = 2.112mm$).**

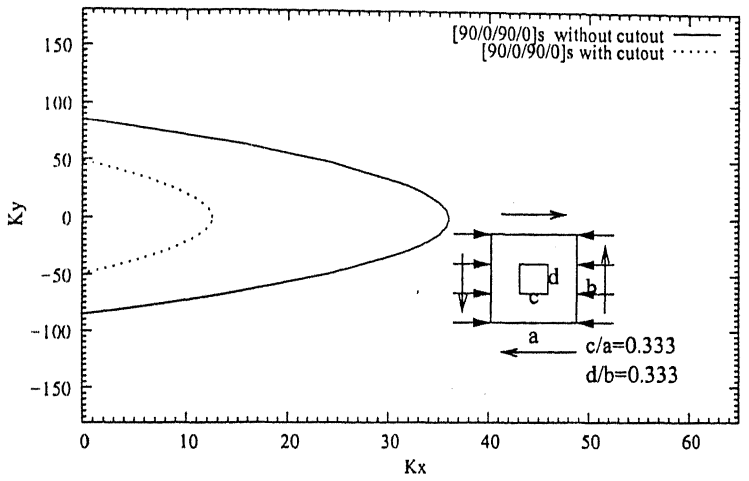

Figure 4.36: **Comparative study of stability envelop for biaxial in-plane compressive and shear loads N_x and N_{xy} with and without cutout, (Material- M2), a/b=1 a/h=100, ($b = 254mm, h = 2.112mm$).**

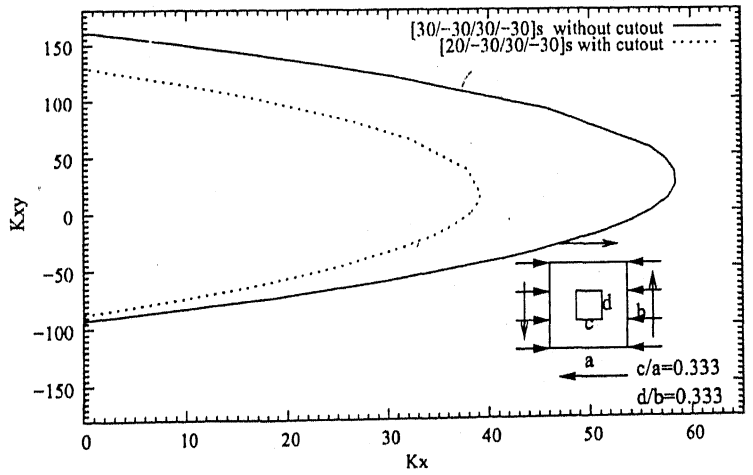

Figure 4.37: **Comparative study of stability envelop for biaxial in-plane compressive and shear loads N_x and N_{xy} with and without cutout,. (Material- M2), a/b=1 a/h=100, ($b = 254mm, h = 2.112mm$).**

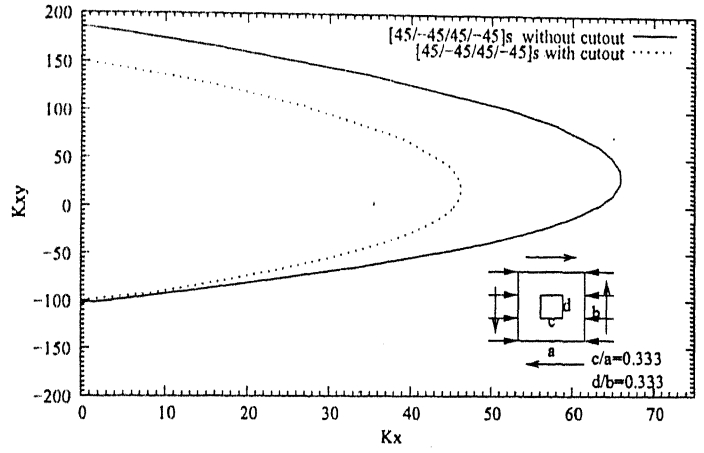

Figure 4.38: **Comparative study of stability envelop for biaxial in-plane compressive and shear loads N_x and N_{xy} with and without cutout, (Material- M2), a/b=1 a/h=100, ($b = 254mm, h = 2.112mm$).**

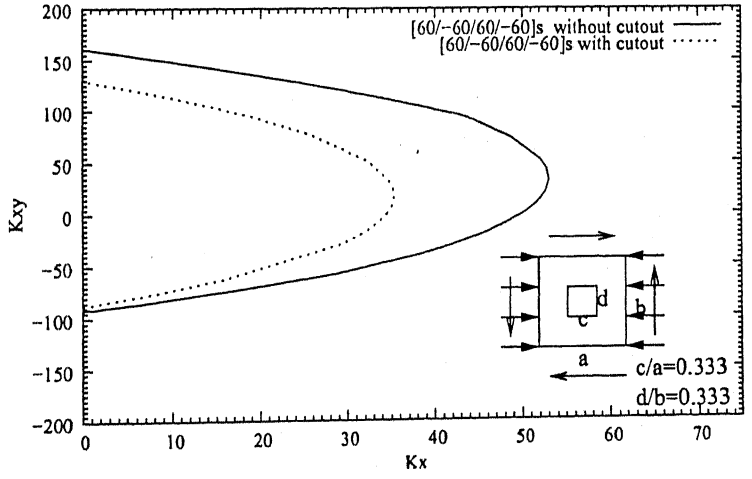

Figure 4.39: **Comparative study of stability envelop for biaxial in-plane compressive and shear loads N_x and N_{xy} with and without cutout, (Material- M2), a/b=1 a/h=100, ($b = 254mm, h = 2.112mm$).**

4.11 Effect of Cutout to Plate Ratio on the Buckling Load of a Laminated Composite Plate.

In this section the effect of cutout to plate ratio on the buckling load of two laminates ($[0/90]_5$ and $[-45/45]_5$) is made. The material properties used are M-2 and the results are plotted for in-plane compressive loading N_x. The plot for $[0/90]_5$ laminate is shown in Fig. 4.40 and that for $[-45/45]_5$ is shown in Fig. 4.41. The figures show the variation of the buckling load for various hole to plate ratio's in X direction with the hole to plate ratio in Y direction. Also the corresponding buckling load for a plate without a cutout is shown in the plots. The following observations can be made from the figures .

- For $[0/90]_5$ laminate the buckling load increases gradually until the hole to plate ratio in Y direction reaches 0.3 for $c/a = 0.1$ and there after it drops down. But for a $[45/-45]_5$ laminate the maximum value of the buckling load occurs when the hole to plate ratio in Y direction reaches 0.38.

- Considering the case when $c/a = 0.2$, its interesting to note that the buckling load exceeds the value without a cutout. The same trend can also be observed with $[45/-45]_5$ laminate. Here the buckling load reaches it peak with $d/b = 0.18$ and there after it comes down. So, for this hole to plate ratio the stiffness of the plate is increasing than that of a plate without a cutout.

- For the remaining hole to plate ratio's, the buckling load gradually drops down for both the laminates.

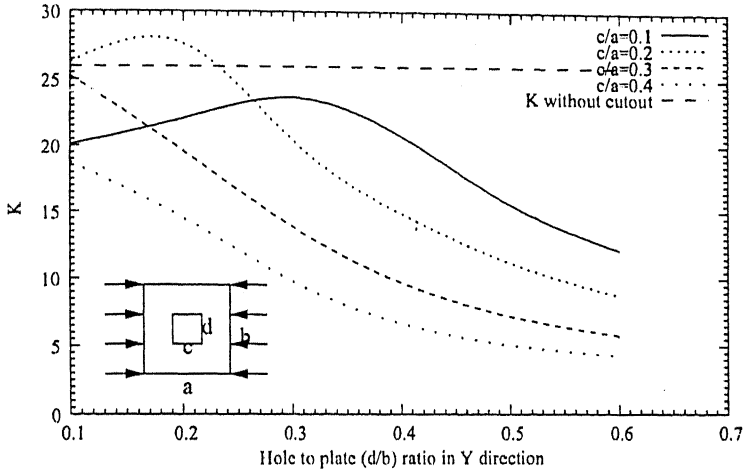

Figure 4.40: **Buckling load vs Hole to plate ratio in Y-direction under in-plane load N_x , (Material- M2), a/b=1 a/h=10**

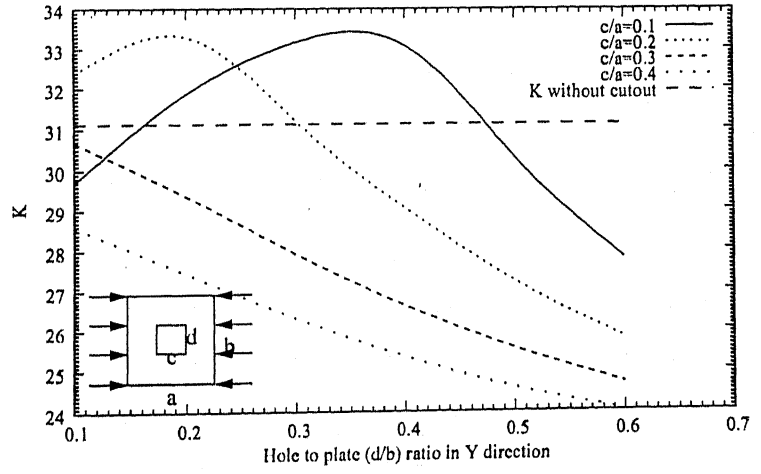

Figure 4.41: **Buckling load vs Hole to plate ratio in Y-direction under in-plane load N_x , (Material- M2), a/b=1 a/h=10**

Chapter 5

Conclusions and Future Scope

5.1 Conclusions

In the present study the initial buckling load of the composite laminates with and without a cutout is studied for different fibre orientation angles, plate aspect ratios and length/thickness ratios. The computations are done for both uniaxial and biaxial loads (both compressive and shear). Interaction curves under the above said loadings are made taking the effects of the cutout. Finite element method is employed to compute the eigen values which are obtained from the finite element solution. The fundamental eigen value corresponds to the initial buckling load of the laminated composite plate.

The following conclusions are made from the present investigation.

- The effect of transverse shear is negligible for thin laminates, but coming to thick plates it has to be duly taken in to account for calculating the buckling load. Hence HSDT should be used for moderately thick and thick plates.
- The effect of laminate orientation angle on the initial buckling load of an antisymmetric laminate decreases with the increase in the length/thickness ratio.
- For thick laminates the effect of laminar orientation angle of antisymmetric laminate on the initial buckling load decreases as the aspect ratio increases.

- For thick laminates the critical fibre orientation angle becomes smaller as the aspect ratio of the laminate increases.

- The buckling load of a laminated plate decreases when a cutout is placed in it at the center. There is a shift in the critical fibre orientation angle for a plate with a cutout.

- Interaction curves for N_x and N_y for a plate without a cutout are linear or piecewise linear. But with a cutout, the linear relationship no longer exists.

- There are some unique points where the laminates carry same amount of buckling load. This combination exists even for a plate with a cutout. But the magnitude of buckling load is considerably reduced when a cutout is placed.

- The stability envelops for combined shear and compressive loadings (N_x and N_{xy}) are symmetric only for a crossly laminate. But for other laminates they are no longer symmetric. The same trend can also be observed for a plate with a cutout .

- There is a decrease in the buckling load of a composite plate when a cutout is placed. But there exists one specific hole to plate ratio where the buckling load exceeds that of a plate without a cutout. So we can say that the stiffness of the plate increases with the material removal.

5.2 Scope for Future Work

The areas which require further study in the future are given below.

- The analysis of plates with multiple cutouts of different geometries and at different locations can be made.

- The laminate orientation angles can be optimized to get the optimistic buckling load.

- Response of laminates with plydrops need to be investigated.

- The present analysis is done taking only linear relationships. So further investigation can be made taking in to effect the non-linear effects.
- Stability analysis of thick laminates with different combinations of thermal/hygroscopic and static in-plane loading.

APPENDIX A

$$\begin{Bmatrix} N_x \\ N_y \\ N_{xy} \\ M_x \\ M_y \\ M_{xy} \\ P_x \\ P_y \\ P_{xy} \\ Q_x \\ Q_y \end{Bmatrix} = \sum_{K=1}^{NL} \begin{bmatrix} [A]_{3\times3} & [B]_{3\times3} & [E]_{3\times3} & [0]_{3\times2} \\ [B]_{3\times3} & [D]_{3\times3} & [F]_{3\times3} & [0]_{3\times2} \\ [E]_{3\times3} & [F]_{3\times3} & [H]_{3\times3} & [0]_{3\times2} \\ [0]_{2\times3} & [0]_{2\times3} & [0]_{2\times3} & [G]_{2\times2} \end{bmatrix}_k \begin{Bmatrix} \epsilon_{0x} \\ \epsilon_{0y} \\ \epsilon_{0xy} \\ k_{0x} \\ k_{0y} \\ k_{0xy} \\ k_{1x} \\ k_{1y} \\ k_{1xy} \\ \gamma_x \\ \gamma_y \end{Bmatrix} \qquad (.1)$$

where,

$$[A]_k = \begin{bmatrix} \bar{Q}_{11}H_1 & \bar{Q}_{12}H_1 & \bar{Q}_{16}H_1 \\ \bar{Q}_{12}H_1 & \bar{Q}_{22}H_1 & \bar{Q}_{26}H_1 \\ \bar{Q}_{16}H_1 & \bar{Q}_{26}H_1 & \bar{Q}_{66}H_1 \end{bmatrix}_k$$

$$[B]_k = \begin{bmatrix} \bar{Q}_{11}H_2 & \bar{Q}_{12}H_2 & \bar{Q}_{16}H_2 \\ \bar{Q}_{12}H_2 & \bar{Q}_{22}H_2 & \bar{Q}_{26}H_2 \\ \bar{Q}_{16}H_2 & \bar{Q}_{26}H_2 & \bar{Q}_{66}H_2 \end{bmatrix}_k$$

$$[D]_k = \begin{bmatrix} \bar{Q}_{11}H_3 & \bar{Q}_{12}H_3 & \bar{Q}_{16}H_3 \\ \bar{Q}_{12}H_3 & \bar{Q}_{22}H_3 & \bar{Q}_{26}H_3 \\ \bar{Q}_{16}H_3 & \bar{Q}_{26}H_3 & \bar{Q}_{66}H_3 \end{bmatrix}_k$$

$$[E]_k = \begin{bmatrix} \bar{Q}_{11}H_4 & \bar{Q}_{12}H_4 & \bar{Q}_{16}H_4 \\ \bar{Q}_{12}H_4 & \bar{Q}_{22}H_4 & \bar{Q}_{26}H_4 \\ \bar{Q}_{16}H_4 & \bar{Q}_{26}H_4 & \bar{Q}_{66}H_4 \end{bmatrix}_k$$

$$[F]_k = \begin{bmatrix} \bar{Q}_{11}H_5 & \bar{Q}_{12}H_5 & \bar{Q}_{16}H_5 \\ \bar{Q}_{12}H_5 & \bar{Q}_{22}H_5 & \bar{Q}_{26}H_5 \\ \bar{Q}_{16}H_5 & \bar{Q}_{26}H_5 & \bar{Q}_{66}H_5 \end{bmatrix}_k$$

$$[H]_k = \begin{bmatrix} \bar{Q}_{11}H_7 & \bar{Q}_{12}H_7 & \bar{Q}_{16}H_7 \\ \bar{Q}_{12}H_7 & \bar{Q}_{22}H_7 & \bar{Q}_{26}H_7 \\ \bar{Q}_{16}H_7 & \bar{Q}_{26}H_7 & \bar{Q}_{66}H_7 \end{bmatrix}_k$$

$$[G]_k = \begin{bmatrix} \bar{Q}_{44}H_8 & \bar{Q}_{45}H_8 \\ \bar{Q}_{45}H_8 & \bar{Q}_{55}H_8 \end{bmatrix}_k$$

in which,

$H_i = \frac{1}{i}\left({z^i}_k - {z^i}_{k-1} \right)$, $i = 1, 2, 3, 4, 5, 7$

and $H_8 = [\{z_k - z_{k-1}\} - \frac{8}{3h^2}\{{z^3}_k - {z^3}_{k-1}\} + \frac{16}{5h^2}\{{z^5}_k - {z^5}_{k-1}\}]$.

also

$$[D_r] = \begin{bmatrix} [A] & [B] & [E] & [0] \\ [B] & [D] & [F] & [0] \\ [E] & [F] & [H] & [0] \\ [0] & [0] & [0] & [G] \end{bmatrix} \qquad (.2)$$

The aforementioned shape functions can be expressed in natural co-ordinates as:

$$\hat{N}_1' = \frac{1}{16}(\xi - 1)^2(-\xi - 2)(\eta - 1)^2(-\eta - 2)$$

$$\hat{N}_2' = \frac{1}{16}(\xi + 1)^2(\xi - 2)(\eta - 1)^2(-\eta - 2)$$

$$\hat{N}_3' = \frac{1}{16}(\xi + 1)^2(\xi - 2)(\eta + 1)^2(\eta - 2)$$

$$\hat{N}_4' = \frac{1}{16}(\xi - 1)^2(-\xi - 2)(\eta + 1)^2(\eta - 2)$$

$$\hat{N}_5' = \frac{1}{16}(\xi - 1)^2(-\xi - 1)(\eta - 1)^2(-\eta - 2)$$

$$\hat{N}_6' = -\frac{1}{16}(\xi + 1)^2(\xi - 1)(\eta - 1)^2(-\eta - 2)$$

$$\hat{N}_7' = -\frac{1}{16}(\xi + 1)^2(\xi - 1)(\eta + 1)^2(\eta - 2)$$

$$\hat{N}_8' = \frac{1}{16}(\xi - 1)^2(-\xi - 1)(\eta + 1)^2(\eta - 2)$$

$$\hat{N}_9' = \frac{1}{16}(\xi - 1)^2(-\xi - 2)(\eta - 1)^2(-\eta - 1)$$

$$\hat{N}_{10}' = \frac{1}{16}(\xi + 1)^2(\xi - 2)(\eta - 1)^2(-\eta - 1)$$

$$\hat{N}_{11}' = -\frac{1}{16}(\xi + 1)^2(\xi - 2)(\eta + 1)^2(\eta - 1)$$

$$\hat{N}_{12}' = -\frac{1}{16}(\xi - 1)^2(-\xi - 2)(\eta + 1)^2(\eta - 1)$$

$$\hat{N}_{13}' = \frac{1}{16}(\xi - 1)^2(-\xi - 1)(\eta - 1)^2(-\eta - 1)$$

$$\hat{N}_{14}' = -\frac{1}{16}(\xi + 1)^2(\xi - 1)(\eta - 1)^2(-\eta - 1)$$

$$\hat{N}_{15}' = \frac{1}{16}(\xi + 1)^2(\xi - 1)(\eta + 1)^2(\eta - 1)$$

$$\hat{N}_{16}' = -\frac{1}{16}(\xi - 1)^2(-\xi - 1)(\eta + 1)^2(\eta - 1)$$

APPENDIX C

The details of $[B_0]$ and $[B_g]$ matrices are as shown:

$$[B_0] = \begin{bmatrix} N_{i,x} & 0 & 0 & 0 \\ 0 & N_{i,y} & 0 & 0 \\ N_{i,y} & N_{i,x} & 0 & 0 \\ 0 & 0 & -N_{i,xx} & 0 \\ 0 & 0 & -N_{i,yy} & 0 \\ 0 & 0 & -2N_{i,xy} & 0 \\ 0 & 0 & 0 & -\frac{4}{3h^2} N_{i,xx} \\ 0 & 0 & 0 & -\frac{4}{3h^2} N_{i,yy} \\ 0 & 0 & 0 & -\frac{8}{3h^2} N_{i,xy} \\ 0 & 0 & 0 & N_{i,x} \\ 0 & 0 & 0 & N_{i,y} \end{bmatrix}_{11\times 64} \tag{.3}$$

and:

$$[B_g] = \begin{bmatrix} 0 & 0 & N_{i,x} & N_{i,x} \\ 0 & 0 & N_{i,y} & N_{i,y} \end{bmatrix}_{2\times 64} \tag{.4}$$

In the above matrices, for columns 1 and 2, $i = 1-12$ (shape functions corresponding to u_0 and v_0) and for columns 3 and 4, $i = 1-16$ (shape functions corresponding to w_b and w_s).

References

[1] J. N. Reddy. An Introduction to Finite Element Method. McGraw-Hill International Editions, Engineering Mechanics Series, 1993.

[2] S. P. Lim, K. H. Lee, S. T. Chow and N. R. Senthilnathan, "Linear and nonlinear bending of shear deformable plates," *Computers and structures, Vol. 30, 1988, pp. 945-952.*

[3] J. M. Whitney. The effect of transverse shear deformation on the bending of laminated plates. *Jnl of Comp Mat* 1969;3:534-547.

[4] J. M. Whitney and N. J. Pagano. Shear deformation in heterogeneous anisotropic plates. *Jnl of Appl Mech* 1970;37:1031-1036.

[5] J. N. Reddy. A Simple higher order theory for laminated composite plates. *Jnl of Appl Mech* 1984;51:745-752.

[6] Gajbir singh. Nonlinear Bending,Vibration and Buckling of Composite Beams and Plates. Ph. D. Thesis, Indian Institute of Technology, Kanpur, March 1993.

[7] Arindam Chakraborty. Stability Analysis of Composite Laminates Using Simple Higher Order Shear Deformation theory. M. Tech. Thesis, Indian Institute of Technology, Kanpur, March 2003.

[8] A.L. Yettram and C.J. Brown. The elastic stability of square perforated plates. *Computers and structures, Vol. 21, 1985, pp.1267-1272.*

[9] Srivatsa KS, Murty AVK. Stability of laminated composite plates with cutouts. *Computers and structures, Vol. 43, 1991, pp.273-279.*

[10] Payal Jain and Aswini Kumar. Postbuckling response of square laminates with a central circular/elliptical cutout. *Computers and structures, Vol. 65, 2003, pp. 179-185.*

[11] D.L. Prabhakara and P.K. Datta. Vibration, buckling and paramteric instability behaviour of plates with centrally located cutouts subjected to in-plane edge loading (Tension and Compression). *Thin-Walled Structures, Vol. 27, 1997, pp. 287-310.*

[12] J. N. Reddy and A. A. Khdeir. Buckling and vibration of laminated composite plates using various plate theories. *AIAA Jnl* 1989;27(12):1808-1817.

[13] Bogner, F. K., Fox, R. L. and Schmit, L. A. The generation of interelement compatible stiffness and mass matrices by the use of interpolation formulas. In: Matrix Methods in Structural Mechanics, Proceeding Conference (AFFDL-TR-66-80), Wright-Patterson A.F.B., Ohio, October 1966. p. 397-444.

[14] Ricardo L. Actis, Barna A. Szabo and Christoph Schwab. Heirarchic models for laminated plates and shells. Computational Methods Appl.Mech.Engineering., 172 (1999) 79-107.

[15] Robert M. Jones. Mechanics of Composite Materials. Scripta Book Company, McGraw-Hill Kogakusha, Ltd. New Delhi, 1975

[16] C. J. Brown, Alan L. Yettram and Mark Burnett. Stability of plates with rectangular holes. *Jnl of Str Engg* 1987;113(5):1111-1116.